Article

SOURCE
DATA

TRANSPARENT
PROCESS

THE
EMBO
JOURNAL

A TRPV1-to-secretagogin regulatory axis controls pancreatic β-cell survival by modulating protein turnover

Katarzyna Malenczyk[1,2], Fatima Girach[1], Edit Szodorai[1], Petter Storm[3], Åsa Segerstolpe[4], Giuseppe Tortoriello[2,†], Robert Schnell[5], Jan Mulder[6], Roman A Romanov[1,2], Erzsébet Borók[7], Fabiana Piscitelli[8], Vincenzo Di Marzo[8], Gábor Szabó[9], Rickard Sandberg[4], Stefan Kubicek[10], Gert Lubec[11,‡], Tomas Hökfelt[2], Ludwig Wagner[12], Leif Groop[3] & Tibor Harkany[1,2,*] (iD)

Abstract

Ca^{2+}-sensor proteins are generally implicated in insulin release through SNARE interactions. Here, secretagogin, whose expression in human pancreatic islets correlates with their insulin content and the incidence of type 2 diabetes, is shown to orchestrate an unexpectedly distinct mechanism. Single-cell RNA-seq reveals retained expression of the TRP family members in β-cells from diabetic donors. Amongst these, pharmacological probing identifies Ca^{2+}-permeable transient receptor potential vanilloid type 1 channels (TRPV1) as potent inducers of secretagogin expression through recruitment of Sp1 transcription factors. Accordingly, agonist stimulation of TRPV1s fails to rescue insulin release from pancreatic islets of glucose intolerant secretagogin knock-out($^{-/-}$) mice. However, instead of merely impinging on the SNARE machinery, reduced insulin availability in secretagogin$^{-/-}$ mice is due to β-cell loss, which is underpinned by the collapse of protein folding and deregulation of secretagogin-dependent USP9X deubiquitinase activity. Therefore, and considering the desensitization of TRPV1s in diabetic pancreata, a TRPV1-to-secretagogin regulatory axis seems critical to maintain the structural integrity and signal competence of β-cells.

Keywords Ca^{2+} signalling; β-cell; diabetes; endocannabinoid; exocytosis
Subject Categories Molecular Biology of Disease; Signal Transduction

Introduction

Life-long maintenance of the cellular integrity of Langerhans islets is critical for biphasic hormone release and therefore adequate responses to environmental and metabolic demands. β-cells produce insulin, and it is their progressive demise that is the causative basis of both type 1 and 2 diabetes (Deng *et al*, 2004; Ize-Ludlow *et al*, 2011). Despite intense research on restorative strategies to facilitate cell turnover or the expansion of the remnant β-cell pool, available solutions amenable to diabetic conditions remain limited. The lack of breakthroughs is particularly concerning when considering the manifold receptor-dependent signalling events modulating β-cell survival.

Changes in intracellular Ca^{2+} levels regulate many cellular processes within pancreatic β-cells, ranging from transcription (German *et al*, 1990), protein folding (Creutz *et al*, 1994; Lievremont *et al*, 1997) and insulin exocytosis (Henquin *et al*, 2002) to the control of cell fate (Skrzypski *et al*, 2015). Translation of Ca^{2+} signals into physiologically meaningful output relies, in part, on Ca^{2+}-sensor proteins, which upon Ca^{2+} binding undergo conformational changes and can phasically activate or inactivate their specific

1   Department of Molecular Neurosciences, Center for Brain Research, Medical University of Vienna, Vienna, Austria
2   Department of Neuroscience, Karolinska Institutet, Stockholm, Sweden
3   Department of Clinical Sciences, Diabetes and Endocrinology CRC, Skåne University Hospital Malmö, Malmö, Sweden
4   Integrated Cardio Metabolic Centre, Karolinska Institutet, Huddinge, Sweden
5   Department of Medical Biochemistry and Biophysics, Karolinska Institutet, Stockholm, Sweden
6   Science for Life Laboratory, Karolinska Institutet, Solna, Sweden
7   Department of Cognitive Neurobiology, Center for Brain Research, Medical University of Vienna, Vienna, Austria
8   Endocannabinoid Research Group, Istituto di Chimica Biomolecolare, Consiglio Nazionale delle Ricerche, Pozzuoli, Naples, Italy
9   Institute of Experimental Medicine, Hungarian Academy of Sciences, Budapest, Hungary
10 CeMM Research Centre for Molecular Medicine, Vienna, Austria
11 Department of Pharmaceutical Chemistry, University of Vienna, Vienna, Austria
12 University Clinic for Internal Medicine III, General Hospital Vienna, Vienna, Austria
    *Corresponding author. Tel: +43 1 40160 34050; Fax: +43 1 40160 934053; E-mail: tibor.harkany@meduniwien.ac.at
    †Present address: Life Technologies, Glasgow, UK
    ‡Present address: Neuroproteomics Laboratory, Science Park, Ilkovicova 8, Bratislava, Slovakia

target partners via protein–protein interactions (Nelson & Chazin, 1998; Shen *et al*, 2008). To be available in sufficient amounts to decode Ca^{2+} signals, the intracellular turnover of Ca^{2+}-sensors themselves may be Ca^{2+} regulated (van Der Luit *et al*, 1999), thus allowing precise control over their activity. Therefore, the coupling of receptor-mediated Ca^{2+} signalling to transcriptional programmes regulating Ca^{2+}-sensor availability in β-cells represents an appealing yet modestly explored niche to integrate β-cell survival and functionality in type 2 diabetes.

Secretagogin is an EF-hand Ca^{2+}-sensor protein, which is amongst the most abundant proteins in pancreatic β-cells (Wagner *et al*, 2000). Primarily, secretagogin is thought to interact with cytoskeletal proteins (Maj *et al*, 2010; Yang *et al*, 2016), soluble *N*-ethylmaleimide-sensitive-factor attachment receptor (SNARE) components (e.g. SNAP-25, synaptobrevins; Rogstam *et al*, 2007; Romanov *et al*, 2015) and cargo proteins (Bauer *et al*, 2011) to modulate regulated insulin exocytosis. Accordingly, secretagogin loss-of-function studies *in vitro* show negative correlation with insulin release (Wagner *et al*, 2000; Hasegawa *et al*, 2013; Yang *et al*, 2016). Secondly, secretagogin has been implicated in the regulation of β-cell proliferation (Wagner *et al*, 2000). Therefore, and even if causality between secretagogin and insulin expression and release exists, the SNARE interactome of secretagogin alone is likely insufficient to chiefly account for the progressive loss of pancreatic β-cells in diabetes. Instead, the analysis of alternative regulatory pathways seems warranted, particularly to map receptor-to-gene transcription axes impacting the Ca^{2+}-dependent regulation of cell turnover.

Here, we combined bulk mRNA expression profiling of pancreatic islets obtained from a human cohort and single-cell RNA-seq from diabetic donors to establish an inverse correlation between secretagogin expression and the incidence of type 2 diabetes. To determine the identity of Ca^{2+}-permeable channels regulating secretagogin function in β-cells, we focused on TRP family members that can fine-tune Ca^{2+}-dependent transcriptional elements. Pharmacological probing of TRP channels revealed that transient receptor potential type 1 vanilloid channels (TRPV1) are particularly poised to induce secretagogin mRNA and protein expression. We then combined *in silico* models, secretagogin promoter assays, biochemistry and mouse genetics to establish that Sp1-dependent promoter activation is causal to TRPV1-mediated secretagogin expression. Next, we generated secretagogin$^{-/-}$ mice that by 6 weeks of age display glucose intolerance, which coincides with the progressive loss of their β-cell mass. By using global proteomics and histochemical tools, we find that Ca^{2+}-bound secretagogin can coordinate protein folding and turnover. Accordingly, secretagogin$^{-/-}$ mice exhibit disrupted protein chaperonin activity and significant endoplasmic reticulum (ER) stress. Likewise, secretagogin mRNA levels in pancreatic islets from human diabetic donors negatively correlate with activating transcription factor 4 (*ATF4*) and CCAAT-enhancer-binding protein homologous protein (*CHOP*) expression. Cellular models and acute genetic manipulations reveal that secretagogin deletion renders its interacting partners, ubiquitin carboxyl-terminal hydrolases (USP9X and USP7) inactive, thus shifting the balance of β-cell proliferation/death towards increased apoptosis. Therefore, a ubiquitously Ca^{2+}-driven TRPV1-to-secretagogin transcriptional axis is suggested as a signal transduction pathway whose deregulation can curtail the

life-long structural integrity and functional competence of pancreatic β-cells.

Results

Secretagogin is a molecular predictor of type 2 diabetes

Secretagogin is a Ca^{2+}-sensor protein, and when silenced *in vitro* negatively couples to insulin secretion (Wagner *et al*, 2000; Hasegawa *et al*, 2013; Yang *et al*, 2016). Secretagogin mRNA and protein expression are preferentially associated with endocrine cell identities, including hormone or neuropeptide-producing cells in brain, pituitary, gastrointestinal tract and pancreas in both human and mouse (Fig EV1A and B; reviewed in: Alpar *et al*, 2012). More specifically, secretagogin immunoreactivity was seen in glucagon$^+$/α-cells, insulin$^+$/β-cells, somatostatin$^+$/δ-cells and pancreatic polypeptide$^+$/PP-cells in the islets of Langerhans in mouse (Fig EV1C). Thus, secretagogin is a ubiquitous cellular mark in the endocrine pancreas. Nevertheless, this study only focuses on dissecting secretagogin function in differentiated β-cells.

Despite *in vitro* probing of its function in exocytosis earlier, the effects of secretagogin deficiency on glucose homoeostasis—particularly in humans—remain unknown. Therefore, we established whether secretagogin could partake in the development of a diabetic phenotype by analysing gene expression data from pancreatic islets of $n = 32$ subjects diagnosed with type 2 diabetes and $n = 170$ healthy controls (Fadista *et al*, 2014). We found a significant negative correlation between secretagogin mRNA expression and the incidence of diabetes ($\log_2 FC = -0.42$, $P = 0.0066$; Fig 1A). Higher secretagogin mRNA expression also predicted lower glycated haemoglobin in blood (HbA1c; $R^2 = 0.059$, $P = 0.0097$; Fig 1A$_1$). Moreover, a significant positive correlation between secretagogin and insulin mRNA expression ($R^2 = 0.2$, $P = 2.7e^{-11}$; Fig 1A$_2$) suggested a role for secretagogin in the hormonal control of glucose metabolism *in vivo*.

TRP channels regulate secretagogin mRNA expression

Ca^{2+}-sensors are regulated by ionic conductances through Ca^{2+} permeable channels, thus allowing their efficient translation of environmental stimuli into adequately-tuned physiological cellular responses (Celio, 1990; Schwaller, 2010). Considering that ion binding of any sensor protein is not restricted to a single cation, we first tested secretagogin's metal ion specificity (the basis for being a "Ca^{2+}-sensor") using recombinant secretagogin (Fig EV2). We demonstrate secretagogin's preference for bivalent members of the Beryllium group (Be, Ca, Mg, Sr) for protein-fold stabilization using the Thermofluor technique (Ericsson *et al*, 2006), which particularly favours Ca^{2+} over Mg^{2+} under quasi-physiological ion concentrations considering its ~100-fold higher affinity for Ca^{2+} (Rogstam *et al*, 2007).

We hypothesized that Ca^{2+} entry could serve as an essential feedback for the expression of this Ca^{2+}-sensor protein. Therefore, we searched for Ca^{2+} permeable channels that (i) can work independently or in tandem with glucose-regulated voltage-gated Ca^{2+} channels, which are lowly expressed in β-cells (Rorsman & Trube, 1986), (ii) their phasic activity can fine-tune β-cell Ca^{2+}
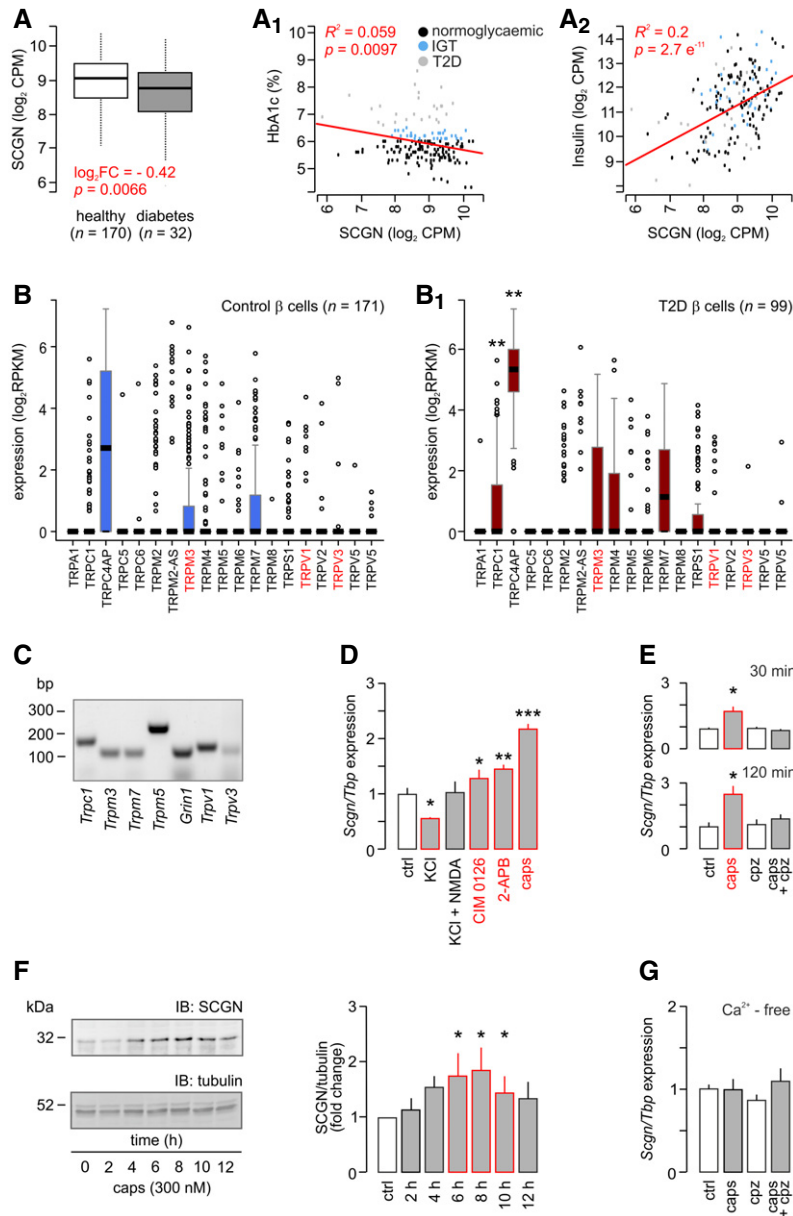
Figure 1. TRP family channels induce secretagogin expression.

A–A2   Transcriptome analysis (bulk) of human (n = 202) pancreatic islets reveals decreased secretagogin (SCGN) expression in patients with type 2 diabetes (T2D; A). A negative correlation between secretagogin expression and the level of glycated haemoglobin (HbA1c) is shown (A1). Conversely, secretagogin mRNA levels positively correlate with insulin expression (A2). Data were presented as $\log_2$ counts per million (CPM). IGT, impaired glucose tolerance. Boxes represent 25th percentiles $\pm$ 90th percentiles, horizontal lines represent median values.

B, B1   Single-cell RNA-seq analysis of TRP family members in β-cells from healthy (n = 6) and type 2 diabetic (n = 4) donors reveals retained TRP expression in β-cells from diabetic subjects. Data were expressed as $\log_2$ reads per kilobase of transcript per million mapped reads (RPKM). Boxes represent 25th percentiles $\pm$ 90th percentiles, horizontal lines represent mean values.

C   Reverse-transcription PCR products of select TRP channels and *Grin1* (encoding NMDA receptor subunit 1) in INS-1E cells.

D   Acute agonist stimulation (30 min) of TRPM3 (CIM 0126; 1 μM), TRPV3 (2-APB; 25 μM) and TRPV1 (capsaicin; caps; 300 nM) promotes secretagogin expression in INS-1E cells with the most pronounced effect evoked by capsaicin. INS-1E cell depolarization with KCl (30 mM, 30 min) decreases secretagogin expression, which was reversed by NMDA.

E   Capsazepine, a TRPV1 antagonist (10 μM), occluded capsaicin-induced secretagogin expression at both 30 and 120 min.

F   Long-term (2–12 h) stimulation of INS-1E cells with capsaicin increases secretagogin protein content. Quantitative data reflect fold changes in SCGN signal intensity normalized to tubulin.

G   Capsaicin fails to increase secretagogin mRNA expression in Ca^{2+}-free media. Representative immunoblots are shown.

Data information: Data were expressed as means $\pm$ s.d. from triplicate experiments (D–G). In (B, B1) **P < 0.01 calculated by Mann–Whitney rank-sum test. In (D–F) ***P < 0.001, **P < 0.01, *P < 0.05 calculated with pairwise comparisons/one-way ANOVA.

Source data are available online for this figure.

signalling, (iii) their ligand levels are changing in type 2 diabetes and (iv) can affect cell proliferation (tissue size) during pancreas development or in pancreatic tumours since secretagogin is re-expressed upon tumorigenic transformation (Wagner *et al*, 2000; Birkenkamp-Demtroder *et al*, 2005; Lai *et al*, 2006). An appealing candidate satisfying the above criteria is the transient receptor potential (TRP) family of channels, which are evolutionarily conserved in the endocrine lineage, Ca^{2+} permeable, and their genetic ablation is implicated in tissue size control (Zhao *et al*, 2013; Riera *et al*, 2014; Malenczyk *et al*, 2015). When screening single-cell RNA-seq data in 270 β-cells from healthy and type 2 diabetic donors (Segerstolpe *et al*, 2016), we find that 17 TRP family members are expressed (> 0.001 RPKM; Fig 1B) with TRPC1 and TRPC4AP levels significantly increased in diabetes. Expression of most other channels was retained in β-cells from diabetic donors. We validated mRNA expression for *Trpc1*, *Trpm3*, *Trpm5*, *Trpm7*, *Trpv1* and *Trpv3* as representatives of the different TRP subfamilies (Clapham *et al*, 2001) as well as for *Grin1* (Marquard *et al*, 2015) in INS-1E cells (Fig 1C). Next, we determined the effect of agonist stimulation of NMDA receptor, TRPM3, TRPV1 and TRPV3 with exogenous ligands (NMDA (20 μM), CIM 0126 (1 μM; Held *et al*, 2015), capsaicin (300 nM) and 2-APB (25 μM; Hu *et al*, 2009), respectively) on secretagogin mRNA expression. We applied 30 mM KCl to induce depolarization-dependent Ca^{2+} influx as control. After 30 min, CIM 0126 ($P < 0.05$), 2-APB ($P < 0.01$) and capsaicin ($P < 0.001$) increased secretagogin mRNA levels with capsaicin producing the most pronounced change (Fig 1D). In turn, KCl-induced passive Ca^{2+} overload reduced secretagogin expression, which was modulated by NMDA co-application (Fig 1D). These data show that temporally confined, receptor-mediated signalling events produce meaningful signals to induce secretagogin transcription.

TRPV1-induced secretagogin accumulation in β-cells is Ca^{2+} dependent

TRPV1s are particularly interesting since they are rapidly activated by anandamide, other endovanilloids and, for example, capsaicin (Di Marzo & De Petrocellis, 2012). In pancreas, both α- and β-cells express rate-limiting enzymes of anandamide metabolism and TRPV1s (Akiba *et al*, 2004; Malenczyk *et al*, 2013, 2015), which have been functionally implicated in the control of the intracellular Ca^{2+} level, insulin secretion and β-cell turnover (Akiba *et al*, 2004; De Petrocellis *et al*, 2007; Riera *et al*, 2014; Malenczyk *et al*, 2015). Anandamide is present in circulating blood, and its levels significantly increase in obesity and type 2 diabetes (Matias *et al*, 2006). In juvenile mouse plasma, we measured anandamide concentrations to be 20.4 ± 8.2 nM, superseding pK_i for anandamide to activate TRPV1s (5.78 nM; Ross *et al*, 2001).

We verified TRPV1 involvement in capsaicin-induced secretagogin mRNA expression (30 and 120 min time-points are shown; $P < 0.05$; Fig 1E) by demonstrating its sensitivity to capsazepine (TRPV1 antagonist, 10 μM) pre-treatment. We could also see the stimulatory effect of capsaicin on protein translation in INS-1E cells (2–12 h; Fig 1F). Finally, we confirmed the role of Ca^{2+} in the transcriptional regulation of secretagogin expression by showing that removal of extracellular Ca^{2+} precluded the TRPV1-dependent

transcription of secretagogin (Fig 1G). Thus, a Ca^{2+}-dependent mechanism might operate downstream from TRPV1 channels to control secretagogin function in β-cells.

TRPV1s recruit Sp1 transcription factors to regulate secretagogin transcription

We then analysed the mouse and human secretagogin promoter *in silico* to predict binding sites for transcription factors potentially involved in its expressional control (Tables EV1 and EV2). Since Ca^{2+} influx seems indispensable to increase secretagogin mRNA content in INS-1E cells, we focused on the Ca^{2+}-dependent transcription factor *Sp1* because its consensus binding sites were detected in the putative secretagogin promoter (−1,400 to +1) in *both* species (Fig 2A and A_1). Notably, Sp1 activity has previously been linked to transmembrane channels permeable for bivalent cations, including TRPV1 (Moon *et al*, 2012).

Acute capsaicin stimulation (300 nM; 30 min) of TRPV1 receptors in INS-1E cells induced the nuclear translocation of Sp1. This response was capsazepine sensitive, confirming TRPV1 involvement ($P < 0.05$ vs. control; Figs 2B–B_2 and EV3A–A_3). Similarly, activation of TRPM3 and TRPV3 led to Sp1 translocation (Fig EV3C–C_6) at magnitudes lesser than for TRPV1, corroborating our observations on secretagogin mRNA expression (Fig 1C). Likewise, TRPV1 stimulation under Ca^{2+}-free conditions occluded Sp1 translocation (Figs 2B$_3$ and EV3B–B_3).

To define the requirement of Sp1 binding to the enhancement of secretagogin transcription, we generated a construct with the full mouse secretagogin promoter (*Scgn*-full, its 1,400 bps 5′ flanking region) driving firefly luciferase in comparison to a construct in which predicted Sp1 binding sites were deleted (*Scgn*-ΔSp1; Fig 2C). Capsaicin (300 nM; 30 min) significantly increased luciferase-induced chemiluminescence in the *Scgn*-full construct ($P < 0.01$ vs. control; Fig 2C$_1$), measured as the ratio of firefly to *Renilla* luciferase activity. In contrast, *Scgn*-ΔSp1 resulted in a substantial decrease in both basal and capsaicin-stimulated luciferase expression and activity ($P < 0.01$ vs. *Scgn*-full; Fig 2C$_1$), demonstrating the critical contribution of Sp1 transcription factors to regulating secretagogin expression.

Secretagogin links TRPV1 activity to regulated insulin exocytosis

We used *Trpv1*$^{-/-}$ mice to confirm Sp1 function downstream from TRPV1s in β-cells *in vivo*. We show significantly reduced total and nuclear Sp1 immunoreactivity ($P < 0.01$ and $P < 0.01$, respectively; Fig 3A–A_3) in *Trpv1*$^{-/-}$ mice relative to wild-type littermates. Coincidently, secretagogin protein ($P < 0.05$; Fig 3B–B_2) and mRNA levels ($P < 0.05$; Fig 3C) were significantly reduced on a *Trpv1*$^{-/-}$ background. Cumulatively, the above data show that endovanilloid signalling in β-cells promoting Ca^{2+} influx via TRPV1s can modulate secretagogin expression through an Sp1-dependent transcriptional mechanism.

Considering that circulating levels of anandamide, the chief endogenous TRPV1 agonist, are increased in type 2 diabetes (Matias *et al*, 2006; Starowicz *et al*, 2008) and lead to TRPV1 desensitization (Zsombok *et al*, 2011; Sanz-Salvador *et al*, 2012; Gao *et al*, 2012), we asked whether reduced secretagogin levels in *Trpv1*$^{-/-}$ mice represent an adaptive response or instead the
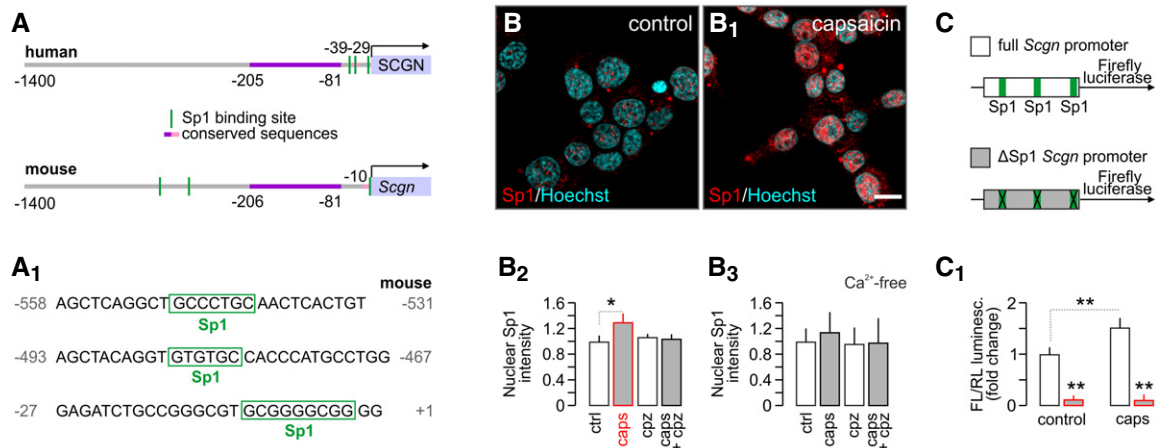
Figure 2. TRPV1 agonism promotes the Sp1-dependent activity of the predicted secretagogin promoter.

A, A₁ *In silico* prediction of *Sp1* transcription factor binding sites within the human and murine secretagogin promoters (up to −1,400 bps). (A₁) Consensus recognition sequences exported from (A).

B–B₃ Capsaicin (caps; TRPV1 agonist; 300 nM for 30 min) induces Sp1 translocation to the nucleus (determined as increased Sp1 immunoreactivity) in INS-1E cells. Representative images are shown. Hoechst 33342 was used as nuclear counterstain. Scale bar = 5 μm. (B₂) This capsaicin effect is blocked by capsazepine (cpz; TRPV1 antagonist, 10 μM). Capsaicin is also ineffective in the absence of extracellular Ca^{2+} (B₃). Representative images for quantitative data are shown in Fig EV3. Data were expressed as means ± s.d. from triplicate experiments with $n \geq 100$ cells/group quantified for (B₂, B₃).

C, C₁ Deletion of predicted Sp1 binding sites in the *Scgn* promoter (C) abrogates basal and capsaicin-induced (300 nM for 30 min) promoter activity defined as a ratio of firefly to *Renilla* luciferase chemiluminescence (3.5 h after stimulation; C₁). Data were expressed as means ± s.d. from triplicate experiments.

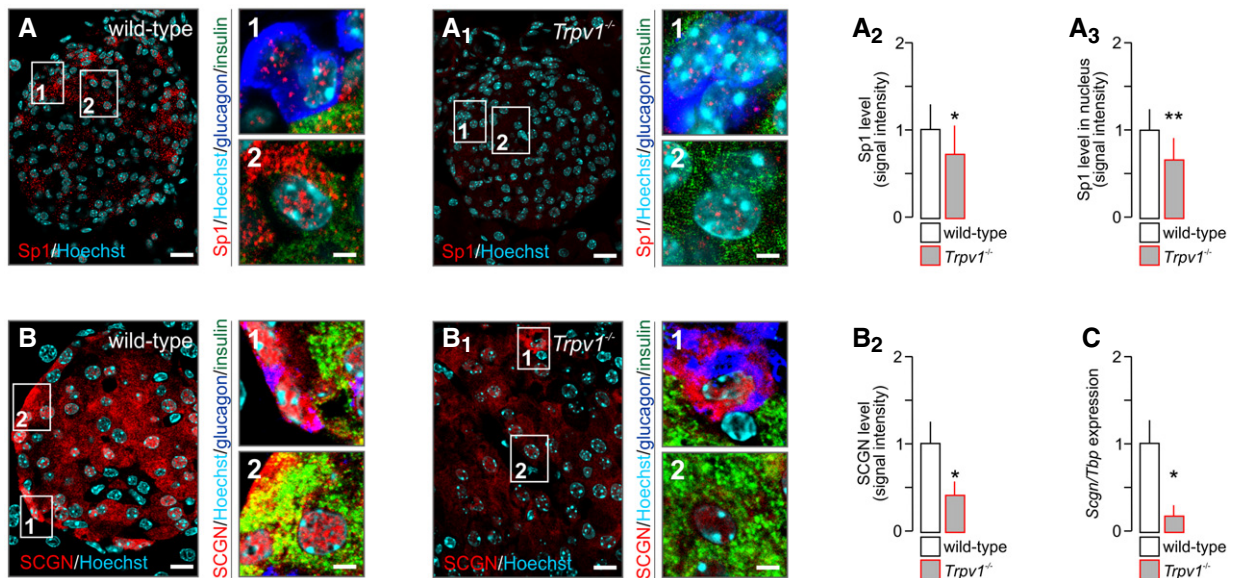Data information: $**P < 0.01$, $*P < 0.05$; Student's t-test (C₁) or one-way ANOVA (B₂).

Figure 3. TRPV1 deletion *in vivo* downregulates secretagogin expression.

A–A₃ Reduced immunoreactivity for total (A₂) and nuclear (A₃) Sp1 in pancreata of $Trpv1^{-/-}$ mice as compared to wild-type controls.

B–B₂ Reduced secretagogin (SCGN) immunoreactivity in pancreata from $Trpv1^{-/-}$ mice. Representative images are shown. Open boxes reflect the general location of numbered insets. Hoechst 33342 was used as nuclear counterstain.

C Likewise, *Scgn* mRNA expression in pancreatic islets isolated from $Trpv1^{-/-}$ mice is significantly decreased.

Data information: Scale bars = 15 μm (A, A₁, B, B₁), 2 μm (numbered inserts). Data were expressed as means ± s.d. from triplicate experiments; $n > 10$ islets from at least three mice/genotype. $**P < 0.01$, $*P < 0.05$; Student's t-test.

loss of secretagogin itself can *per se* precipitate diabetes and modulate TRPV1 signalling. In cultured INS-1E cells, we found that acute siRNA silencing of secretagogin increased TRPV1

protein levels ($P < 0.05$; Figs 4A and EV4A and B). Nevertheless, TRPV1 phosphorylation at its Ser[800] residue did not change (as the ratio of total TRPV1; Fig 4A) suggesting that excess
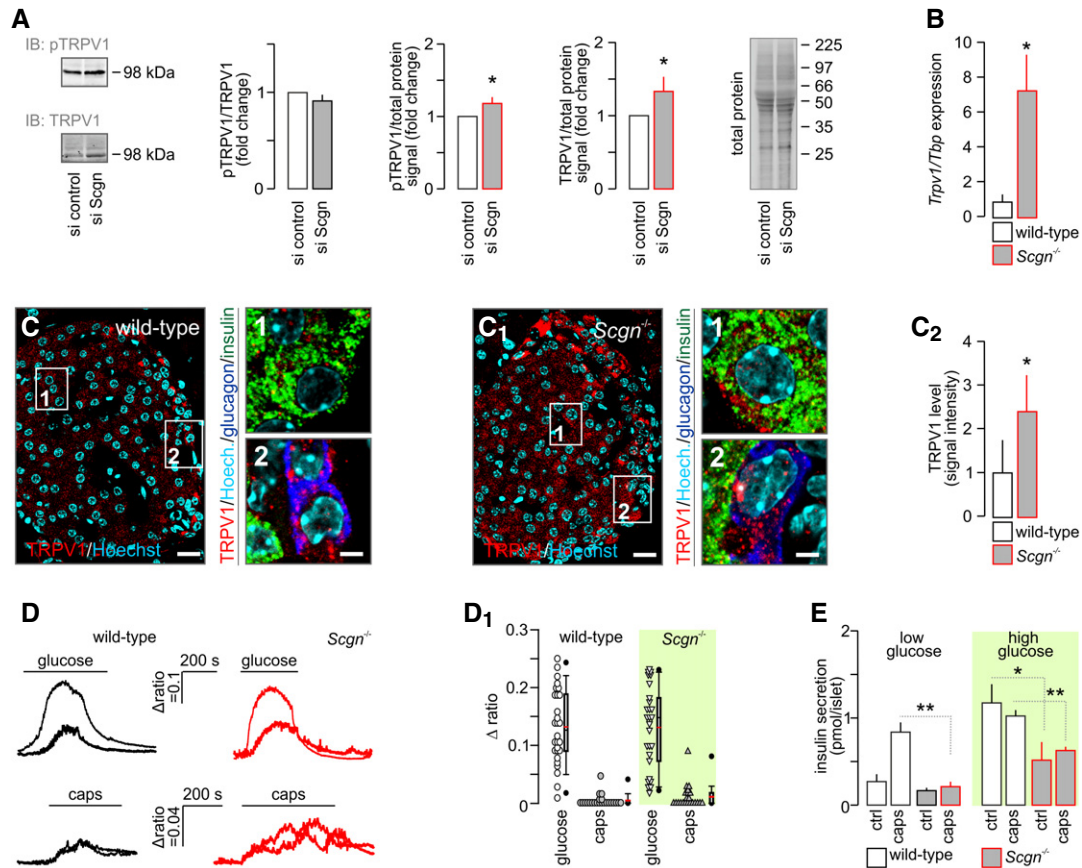
Figure 4. Compensatory upregulation of TRPV1 expression is insufficient to rescue insulin secretion in secretagogin knock-out mice.

A   *Scgn* silencing in INS1-E cells does not affect TRPV1 phosphorylation (expressed as pTRPV1/TRPV1) despite significantly increasing total TRPV1. Total protein dye-labelling was used as control. A representative immunoblot is shown. Quantitative data were expressed as fold changes in signal intensity vs. control and normalized to total protein. Data were expressed as means ± s.d. from triplicate experiments.

B   *Trpv1* mRNA expression in secretagogin knock-out (*Scgn*$^{-/-}$) mice. Data were expressed as means ± s.d. from triplicate experiments.

C–C$_2$ Histochemical detection of TRPV1s in pancreatic islets of *Scgn*$^{-/-}$ mice confirmed their increased amounts relative to wild-type littermates (C$_2$). Representative images are shown. Hoechst 33342 was used as nuclear counterstain. Scale bars = 15 μm and 2 μm (numbered inserts). Quantitative results were expressed as means ± s.d. from triplicate experiments; n > 10 islets (C–C$_2$).

D, D$_1$ In dissociated islets from *Scgn*$^{-/-}$ and wild-type mice, β-cells were identified by their Ca^{2+} responses to 16 mM glucose (upper traces). Subsequent bath application of capsaicin (caps; 300 nM) barely mobilized intracellular Ca^{2+} in β-cells from either genotype (bottom traces). (D$_1$) Quantitative analysis of glucose- and capsaicin-induced Ca^{2+} responses in wild-type and *Scgn*$^{-/-}$ β-cells are shown as dot density plots combined with box plots representing medians and 10th, 25th, 70th and 90th percentiles. Red lines within box plots represent mean and black median values. Peak values during the first 100 s (for capsaicin) or 300 s (for glucose) stimulation were plotted. Mann–Whitney rank-sum test failed to reveal statistically significant differences between wild-type and *Scgn*$^{-/-}$ samples for either stimulation.

E   Capsaicin (300 nM) is ineffective in potentiating basal (low glucose) or glucose-stimulated insulin secretion from pancreatic islets isolated from *Scgn*$^{-/-}$ mice. Data were expressed as means ± s.d. from n = 30 islets (E) from at least three mice/genotype.

Data information: **$P < 0.01$, *$P < 0.05$; Student's t-test (A, B, C$_2$) or pairwise comparisons/one-way ANOVA (E).
Source data are available online for this figure.

TRPV1s brought about by secretagogin knock-down do not confer gain-of-function. Next, we generated secretagogin$^{-/-}$ mice (for histological validation of protein loss see: Fig EV4C–E). Notably, secretagogin$^{-/-}$ mice present > sixfold increase in *Trpv1* mRNA expression ($P < 0.05$; Fig 4B), as well as elevated TRPV1 protein levels in pancreatic islets ($P < 0.05$), particularly in β-cells (Fig 4C–C$_2$). Therefore, we used Ca^{2+} imaging to establish whether surplus TRPV1s are functionally competent or, alike our *in vitro* observations (Fig 4A), are signal deficient. Ca^{2+} imaging in dissociated pancreatic islets showed no difference in either glucose (16 mM) or capsaicin (300 nM)-stimulated Ca^{2+} influx between secretagogin$^{-/-}$ and wild-type β-cells (Fig 4D and D$_1$). Furthermore, and despite the upregulation of TRPV1s, capsaicin, (300 nM) stimulation of pancreatic islets isolated from secretagogin$^{-/-}$ mice was insufficient to potentiate basal (2.75 mM glucose) or rescue glucose-induced insulin release (16.5 mM glucose; both $P < 0.01$ vs. wild type; Fig 4E). Cumulatively, our data suggest that secretagogin acting downstream of Ca^{2+} influx is an essential effector linking TRPV1 activity and glucose metabolism to regulated insulin exocytosis in β-cells, and whose loss can stem insulin release even in the presence of excess TRPV1s.
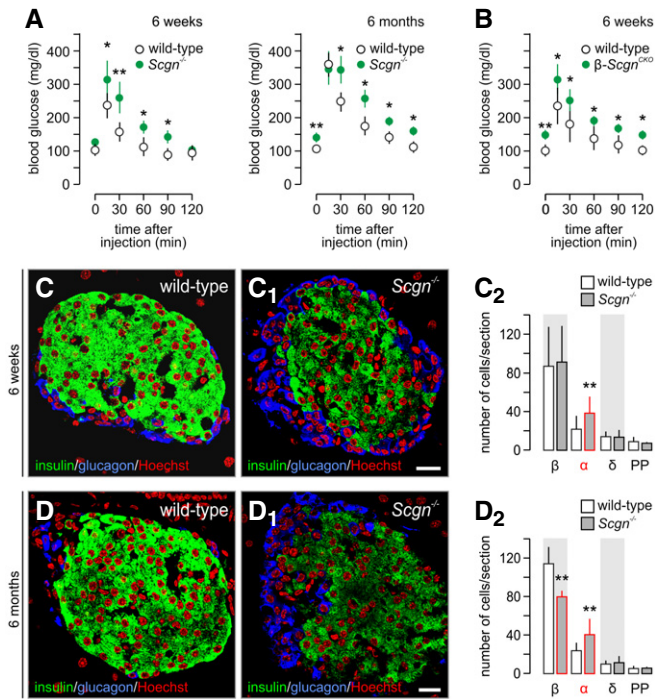
Figure 5. Secretagogin$^{-/-}$ mice develop progressive glucose intolerance and loss of β-cells.

A   Glucose intolerance in secretagogin$^{-/-}$ (*Scgn$^{-/-}$*) mice at 6 weeks of age (*left*). Six-month-old *Scgn$^{-/-}$* mice have a pre-diabetic profile of glucose utilization (*right*), including significantly elevated fasting blood glucose levels. *n* = 6 animals/genotypes/age was used.

B   Elevated fasting blood glucose levels and impaired glucose clearance in β-*Scgn^{CKO}* was observed at 6 weeks of age. *n* = 6 mice/genotype.

C–C$_2$ At the age of 6 weeks, pancreatic islets of *Scgn$^{-/-}$* mice contain an increased number of α-cells in conjunction with unchanged β-cell numbers (C$_2$).

D–D$_2$ At the age of 6 months, however, a significant decrease in β-cells together with persistent α-cell hyperplasia was seen in *Scgn$^{-/-}$* mice relative to wild-type littermates. Representative images are shown. Hoechst 33342 was used as nuclear counterstain (pseudo-coloured in red).

Data information: Scale bars = 15 μm. Data were expressed as means ± s.d. from *n* = 30 islets/group from three mice/genotype were quantified (C–D$_2$). **P < 0.01, *P < 0.05; Student's *t*-test (C$_2$, D$_2$) or one-way ANOVA (A, B).

Secretagogin$^{-/-}$ mice develop progressing glucose intolerance

We went on to test whether secretagogin loss-of-function may be causal to a diabetic phenotype *in vivo*. Indeed, secretagogin$^{-/-}$ mice at both 6 weeks and 6 months of age were glucose intolerant as shown by their attenuated blood glucose clearance (Fig 5A). Moreover, secretagogin$^{-/-}$ mice at 6 months of age presented significantly elevated fasting blood glucose levels (*P* < 0.01; Fig 5A). Notwithstanding, secretagogin$^{-/-}$ mice presented no change in their body weight relative to their wild-type littermates (17.6 ± 1.5 g [secretagogin$^{-/-}$] vs. 17.3 ± 1.7 g [wild type] at 6 weeks and 28.7 ± 3.5 g [secretagogin$^{-/-}$] vs. 28.5 ± 3.7 g [wild type] at 6 months). We then generated β-cell-specific secretagogin$^{-/-}$ mice (*Ins1*-Cre^{ERT}::secretagogin$^{floxed/floxed}$; "β-*Scgn^{CKO}*") to confirm that the detrimental effect of secretagogin loss on glucose metabolism relies specifically on β-cell dysfunction. β-*Scgn^{CKO}* mice lacked

detectable immunoreactivity for secretagogin in > 80% of β-cells 1 week after daily tamoxifen administration (*P* < 0.001; Fig EV4F–H) and presented both elevated fasting blood glucose levels (*P* < 0.01; Fig 5B) and significantly attenuated blood glucose clearance (Fig 5B). Next, we found that pancreatic islets from secretagogin$^{-/-}$ mice, unlike those of their wild-type littermates, were insensitive to glucose (*P* < 0.05 vs. wild type) or KCl stimulation (*P* < 0.01 vs. wild type) *ex vivo* (Fig EV5A). These data were supported by decreased insulin mRNA expression (*P* < 0.01; Fig EV5B), decreased intensity of insulin immunoreactivity in individual β-cells (at both 6 weeks and 6 months, *P* < 0.05; Fig EV5C) and reduced total insulin content in pancreatic islets (*P* < 0.05; Fig EV5D) in secretagogin$^{-/-}$ mice. Disrupted insulin production in secretagogin$^{-/-}$ mice was also suggested by the reduced number of insulin granules in β-cells (*P* < 0.01; Fig EV5E–E$_2$) with a particularly notable effect on the number of docked vesicles (in direct contact with the plasma membrane of β-cells; *P* < 0.001; Fig EV5E$_3$). These data together with previous *in vitro* interaction analyses of secretagogin and cytoskeletal proteins (tubulin and molecular motors of axonal traffic; Maj *et al*, 2010; Bauer *et al*, 2011), as well as components of the exocytosis machinery (Rogstam *et al*, 2007; Romanov *et al*, 2015) unequivocally place secretagogin within the SNARE complex.

When assaying the number of cell types within pancreatic islets of both 6-week and 6-month-old secretagogin$^{-/-}$ mice, we found an age-dependent β-cell loss, which was accompanied with α-cell hyperplasia (Fig 5C and D). The number of δ- and PP-cells remained unchanged at either time point. Since α-to-β-cell imbalance is a principal cause of progressive glucose intolerance and diabetes (Deng *et al*, 2004), a phenotype secretagogin$^{-/-}$ mice exhibit by 6 months of age (*P* < 0.01 vs. wild type at 6 months of age, Fig 5C–D$_2$), we tested whether β-cell loss is a surrogate of secretagogin loss-of-function or instead, secretagogin directly controls β-cell survival and turnover.

Secretagogin modulates protein folding and degradation through protein–protein interactions

Considering the abundance of secretagogin on, for example, ER membranes (Romanov *et al*, 2015; Hanics *et al*, 2017), we screened possible protein–protein interactions unrelated to either the cytoskeleton or SNARE assembly. By using His$_6$-tagged recombinant secretagogin in the presence of Ca^{2+} (100 μM), we precipitated putative interacting partners from INS-1E cells and identified their amino acid sequences by mass spectrometry. We retained canonical interacting proteins participating in vesicle-mediated transport, exocytosis and cytoskeletal organization as positive controls (Fig 6A, Table EV3). Here, we focused on captured proteins controlling protein folding and (de-)ubiquitination (Fig 6B) since disrupted protein maturation is particularly detrimental for secretory cells and could lead to ER stress and eventual cell death (Fig 6C). When annotating secretagogin's interacting partners functionally grouped as those with "protein folding" involvement, we find members of the chaperonin-containing complex (CCT; Fig 6B, Table EV3), known to assist cytoplasmic proteins including actin, tubulin, p53 and c-Myc to acquire their native and functionally active conformations (Grantham *et al*, 2002; Koch *et al*, 2007; Lin *et al*, 2012; Trinidad *et al*, 2013). As such, we then probed T-complex protein 1
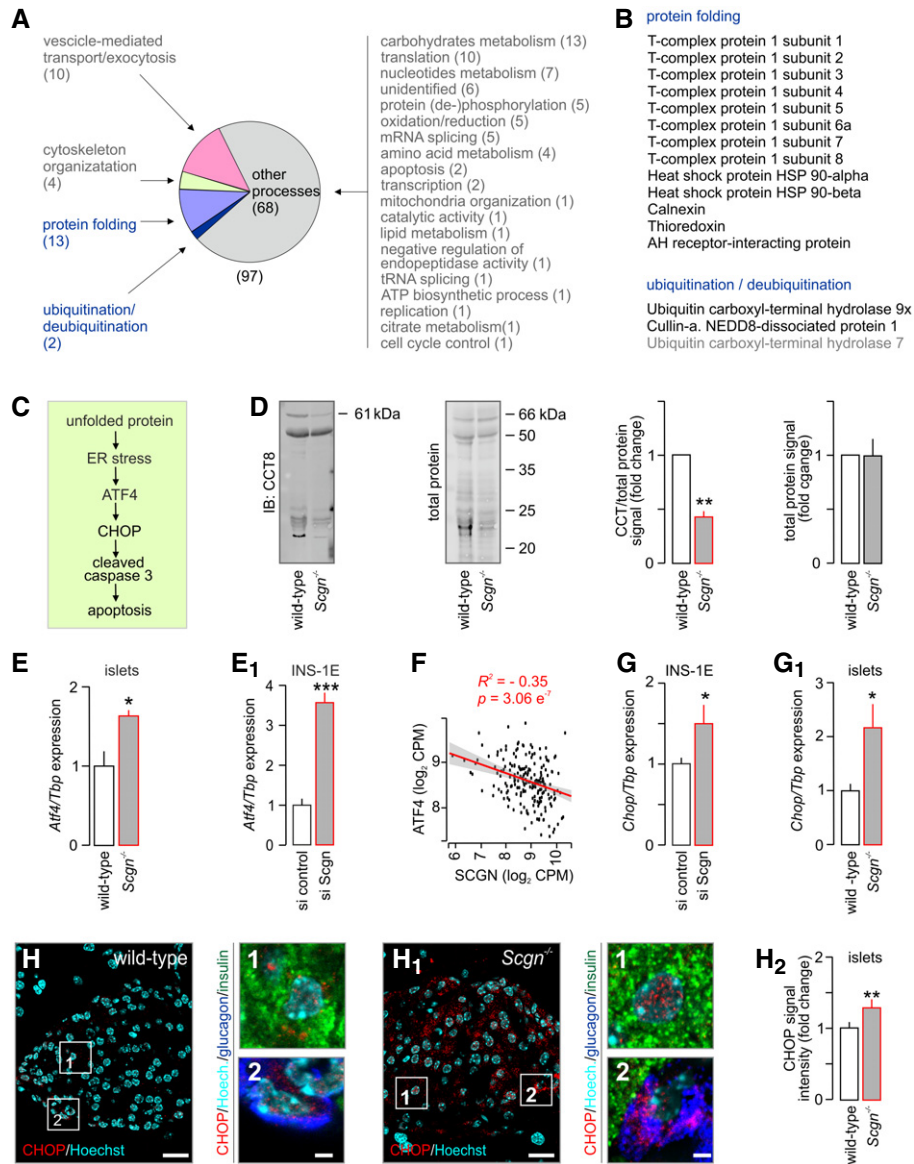
Figure 6. Secretagogin interacts with members of the protein folding machinery to control endoplasmic reticulum homoeostasis.

A   Proteins identified as molecular interactors when using purified His$_6$-tagged secretagogin as bait include (by GO function determination) those for protein folding, vesicle-mediated transport, exocytosis as well as protein (de-)ubiquitination. Bracketed numbers refer to the number of proteins per GO cluster. "Other processes" refer to those, which were not analysed in detail. Nevertheless, the identity, discovery rate and peptide fragmentation data for *all* interacting proteins from our LC-MS/MS analyses are listed in Table EV3.

B   List of interacting partners involved in protein folding and protein ubiquitination/deubiquitination.

C   Schema of predicted steps triggering β-cell death upon unfolded protein response when genetically ablating secretagogin. Decreased protein folding in β-cells is posited to induce endoplasmic reticulum (ER) stress, expression *of Atf4* transcription factor and the pro-apoptotic protein CHOP, leading to the activation of caspase 3 and, ultimately, apoptotic cell death.

D   The level of T-complex protein 1 subunit 8 (CCT8) is significantly decreased in pancreatic islets isolated from *Scgn*$^{-/-}$ mice, as compared to wild-type controls. Left: Representative immunoblot with adjacent Cy5-labelled total protein control are shown. Right: Fold change in CCT8 and total protein in *Scgn*$^{-/-}$ pancreata vs. wild-type littermates. Data are expressed as means $\pm$ s.d. from $n = 3$ mice/genotype.

E, E$_1$ *Atf4* expression is significantly increased in pancreatic islets isolated from *Scgn*$^{-/-}$ mice, as compared to wild-type controls (E) and upon silencing of secretagogin expression (si Scgn) in INS-1E cells (E$_1$). Data represent means $\pm$ s.d. from triplicate experiments.

F   Secretagogin mRNA levels are negatively correlated with ATF4 expression in human pancreatic islets. Means $\pm$ s.d. log$_2$ counts per million (CPM) are shown.

G, G$_1$ mRNA expression of the pro-apoptotic protein *Chop* is significantly increased in INS-1E cells upon secretagogin silencing (G) and in pancreatic islets isolated from *Scgn*$^{-/-}$ mice (G$_1$). Data were normalized to those in control/wild type in triplicate experiments (G) or $n = 3$ mice/genotype (G$_1$) and expressed as means $\pm$ s.d.

H–H$_2$ Increased CHOP immunoreactivity in pancreatic islets of *Scgn*$^{-/-}$ mice as compared to wild-type controls. Representative images are shown. Hoechst 33342 was used as a nuclear counterstain. Scale bars = 15 μm, and 2 μm in numbered insets. (H$_2$) Quantitative data are expressed as means $\pm$ s.d. $n = 20$ islets from 3 mice/genotype were analyzed.

Data information: ***$P < 0.001$, **$P < 0.05$, *$P < 0.05$ by Student's *t*-test.

subunit 8 (CCT8) in pancreatic islets of secretagogin$^{-/-}$ mice and verified its levels to be significantly reduced (Fig 6D).

Additionally, mRNA expression of *Atf4*, a typical marker of ER stress (Harding *et al*, 2003), was significantly increased in islets from secretagogin$^{-/-}$ mice relative to wild-type littermate controls ($P < 0.05$; Fig 6E). We validated the above data as being predictive, rather than auxiliary to progressive diabetes in our secretagogin$^{-/-}$ model, by acute siRNA silencing of secretagogin expression in INS-1E cells (Fig EV4A and B). These experiments (48 h survival after siRNA exposure) confirmed significantly increased *Atf4* RNA expression ($P < 0.001$; Fig 6E$_1$). If reduced secretagogin expression induces ER stress then one can hypothesize a negative correlation between secretagogin and *ATF4* mRNA levels in human diabetic subjects. Indeed, we found a negative correlation in human pancreatic islets ($R^2 = -0.35$, $P < 0.001$; Fig 6F) emphasizing a likely mechanistic link between secretagogin loss-of-function and ensuing ER stress.

Unresolved ER stress and the decreased stability of proteins affecting the cell cycle may lead to apoptosis (Suzuki *et al*, 2001; Yan *et al*, 2014). Since the number of β-cells in pancreatic islets of secretagogin$^{-/-}$ mice is significantly reduced when compared to wild-type littermates (Fig 5D–D$_2$), we analysed the effect of secretagogin deficiency on the level of CHOP (Fig 6C), which mediates apoptosis (Matsumoto *et al*, 1996). *Chop* mRNA expression was significantly upregulated in both INS-1E cells upon secretagogin knock-down ($P < 0.05$; Fig 6G) and in secretagogin$^{-/-}$ islets ($P < 0.05$; Fig 6G$_1$) relative to their respective controls. These data were extended by showing significantly increased CHOP immunoreactivity in pancreatic islets from secretagogin$^{-/-}$ mice ($P < 0.01$; Fig 6H–H$_2$) to suggest that ER stress-related cell death is the likely cause of β-cell loss in secretagogin$^{-/-}$ mice.

Secretagogin interacts with USP9X in β-cells to control cell survival

Impaired protein folding, the primary cause of ER stress in β-cells, is resolved by increased protein degradation through ubiquitination (Allen *et al*, 2004). Acute silencing of secretagogin expression increased the level of ubiquitinated proteins (total) in INS-1E cells by ~50%, equivalent to that of the proteasome inhibitor MG132 (10 μM, 6 h; Fig 7A). However, and contrasting the effect of MG132, secretagogin knock-down did not increase the total protein content of INS-1E cells (Fig 7A$_1$), suggesting either a reduced rate of protein translation or accelerated proteasomal degradation. Our interactome profiling (Fig 6A and B) suggested that Ca^{2+}-bound secretagogin could selectively interact with the ubiquitin carboxyl-terminal hydrolase USP9X, and possibly USP7. Secretagogin's interaction with both USP9X and USP7 was first validated by pull-down with His$_6$-tagged secretagogin followed by immunoblot detection (Fig 7B). Secondly, we found a significant correlation between secretagogin and USP9X mRNA expression in our human cohort ($R^2 = 0.21$, $P < 0.001$; Fig 7C) lending further support to functional interactions. Subsequently, we hypothesized that secretagogin's interaction with ubiquitin carboxyl-terminal hydrolases could prime their deubiquitinating/protein stabilizing activity (with enzymatic activity being reduced on null backgrounds). We tested this concept by detecting known USP9X and USP7 substrates involved in cell cycle control: p53, Mdm2, Mcl-1 (Li *et al*, 2002; Schwickart *et al*,

2010). As such, secretagogin knock-down produced a pronounced decrease in p53 levels in INS-1E cells (Figs 7D and EV6A), validating that secretagogin could interact with USP9X, and thus modulate its activity.

To test the direct output of these changes on cell survival, we assayed Ki67 and cleaved caspase 3, markers of cell proliferation and apoptotic cell death, respectively, in INS-1E cells after secretagogin knock-down. Secretagogin silencing significantly decreased the number of Ki67$^+$ INS-1E cells ($P < 0.01$; Fig EV6B–B$_2$). Simultaneously, the number of cleaved caspase 3$^+$ INS-1E cells significantly increased ($P < 0.05$; Fig EV6C–C$_2$). Next, we asked whether inhibition of protein degradation could rescue the detrimental effect of secretagogin knock-down on INS-1E cell survival. We found that lactacystin (5 μM, 6 h), a proteasome inhibitor, significantly decreased the number of apoptotic INS-1E cells which first underwent secretagogin silencing ($P < 0.01$ vs. siRNA without lactacystin; Fig 7E–E$_4$), which confirmed secretagogin's role in the USP9X-mediated modulation of protein turnover to impact β-cell survival (Fig 7F).

Discussion

Our study identifies TRPV1 signalling converging onto secretagogin expression as an important regulatory axis for both β-cell secretory function and survival. Combining single-cell RNA-seq in human β-cells, studies in the INS-1E cell line *in vitro*, *Trpv1* and secretagogin knock-out mouse models and the bulk analysis of gene expression in islets of a human cohort, we show that impairment of this signalling pathway precipitates both molecular and pathophysiological hallmarks of type 2 diabetes, that is impaired insulin secretion (Pfeifer *et al*, 1981), ER stress (Araki *et al*, 2003) and progressive loss of β-cell mass (Butler *et al*, 2003). We specifically demonstrate that TRPV1 signals through Sp1 to enhance secretagogin promoter activity with resultant increases in secretagogin levels providing a molecular check-point for protein folding and deubiquitination. Thus, we identify a hierarchical signalling cascade that can operate in parallel with secretagogin modulation of the SNARE (exocytosis) machinery, and ensure fundamentally different cellular consequences.

Ca^{2+}-sensor proteins are known to assist in protein folding, maintain ER homoeostasis and control cell fate (Heit *et al*, 2006; Bollo *et al*, 2010). Calcineurin has been shown to modulate β-cell proliferation and survival in humans and rodents (Heit *et al*, 2006; Soleimanpour *et al*, 2010; Goodyer *et al*, 2012). Mice with β-cell-specific deletion of calcineurin are reported to develop age-dependent type 2 diabetes due to a decrease in insulin production and loss of β-cell mass (Heit *et al*, 2006). The mechanism of calcineurin's action in the control of β-cell fate depends on the transcriptional regulation of insulin receptor substrate (*Irs2*; Shirakawa *et al*, 2013) and is clearly different from the action of secretagogin shown here. Despite calmodulin-dependent signalling being essential for both proliferation and apoptosis in many cellular niches (Rasmusen & Means, 1990; Yu *et al*, 2002), its overexpression in β-cells has been linked to impaired insulin secretion, β-cell loss and diabetes (Yu *et al*, 2002). Opposing roles of secretagogin and calmodulin in the control of β-cell turnover are in line with opposite changes in their protein levels seen in diabetic animal models
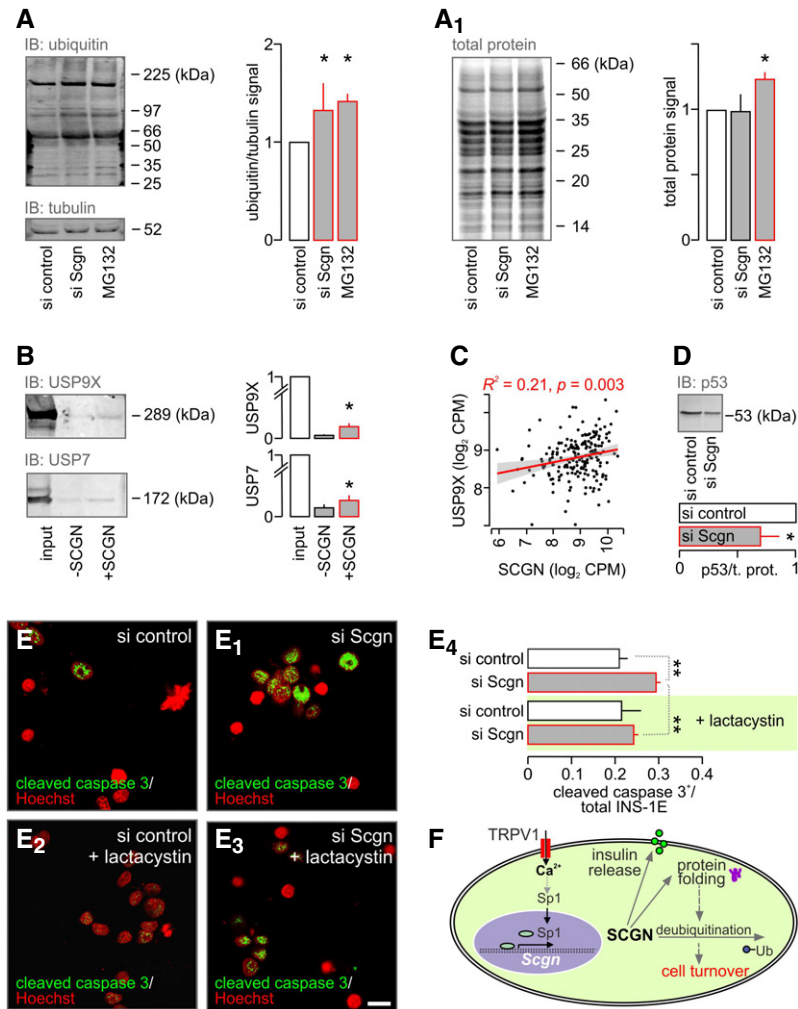
Figure 7. Secretagogin regulates β-cell turnover through modulating protein deubiquitination.

A, A₁   (A) Accumulation of ubiqitinated proteins in INS-1E cells with siRNA-mediated secretagogin knock-down. MG132 (10 µM, 6 h), a proteasome inhibitor, was used as a positive control. (A₁) In contrast to MG132, secretagogin silencing does not alter the total protein level.

B   Ubiquitin carboxyl-terminal hydrolases USP9X and USP7 remained in the eluted fraction upon pull-down with His₆-tagged secretagogin, suggesting protein–protein interaction.

C   USP9X mRNA expression positively correlates with the level of secretagogin mRNA in human pancreatic islets.

D   Impaired activity of USP9X and USP7 upon secretagogin knock-down is validated by the decreased level of USP target protein p53, one of their molecular targets (Li *et al*, 2002). Total protein level is shown in Fig EV6.

E–E₄   Proteasome inhibition by lactacystin (5 µM, 6 h) with concomitant siRNA-mediated secretagogin knock-down significantly reduces the number of cleaved caspase 3⁺ (apoptotic) INS-1E cells. Representative images are shown. Hoechst 33342 was used as a nuclear counterstain (pseudo-coloured in red). Scale bar = 5 µm.

F   Proposed mechanism of the upstream regulation of secretagogin (SCGN) expression to determine β-cell survival. TRPV1-mediated increase in intracellular Ca^{2+} promotes the translocation of Sp1 to the nucleus to induce *Scgn* transcription. SCGN not only participates in insulin secretion but also controls protein folding and cell turnover by interacting with ubiquitin carboxyl-terminal hydrolases.

Data information: Quantitative analysis of immunoblots show fold changes in signal intensity and are normalized to controls. Data were expressed as $\log_2$ counts per million (CPM; in C) or means ± s.d. from triplicate experiments (in A, A₁, B, D and E₄). $n = 202$ (C), $n = 3$ mice/genotype (D), $n \geq 100$ cells/group (E–E₄); **$P < 0.01$, *$P < 0.05$. Student's t-test (D) or one-way ANOVA (A–B, E₄).
Source data are available online for this figure.

(Bazwinsky-Wutschke *et al*, 2010). Moreover, increased levels of calmodulin observed in diabetes could itself impair secretagogin expression, since Ca^{2+}-dependent interaction between calmodulin and the C-terminus of TRPV1 has been shown to promote TRPV1 desensitization and decrease ligand-induced Ca^{2+} currents (Numazaki *et al*, 2003). Thus, secretagogin can be viewed as a

"master switch" amongst Ca^{2+}-sensors that ultimately determines cell fate irrespective of the molecular identity of upstream or secondarily interacting Ca^{2+}-sensor and/or Ca^{2+} buffer proteins.

Under metabolic stress, the proper function of protein chaperones and efficient unfolded protein response signalling are essential coping mechanisms that protect β-cells from apoptosis (Allen *et al*,

2004). Secretagogin's interaction with the chaperonin-containing complex, and a decreased CCT8 protein level in pancreatic islets of secretagogin$^{-/-}$ mice implicate secretagogin in participating in the regulation of protein folding. Importantly for this study, the activity of chaperonins is essential for many cytoskeletal proteins including α- and β- actin, α-, β- and γ-tubulin, and cell cycle regulators, that is p53 to acquire their functional conformation (Dekker *et al*, 2008; Trinidad *et al*, 2013). Considering a crucial role of cytoskeletal components in insulin transport and exocytosis in β-cells (Henquin *et al*, 2012), misfolding of such proteins may be a key factor behind impaired insulin secretion in secretagogin$^{-/-}$ pancreatic islets.

Protein ubiquitination/deubiquitination and the proteasome machinery are crucial to control numerous functions in β-cells including insulin secretion and the cell cycle (Ardestani *et al*, 2014; Sugawara *et al*, 2014; Suriben *et al*, 2015). Protein degradation can directly (e.g. by the control of Mcl-1, p53, cyclins or caspases; Glotzer *et al*, 1991; Suzuki *et al*, 2001; Li *et al*, 2002; Yan *et al*, 2014) or indirectly (e.g. by removing misfolded proteins and decreasing ER overload; Sugawara *et al*, 2014) regulate cell fate. Impairment in the ubiquitin-proteasome system in pancreatic islets has been directly linked to β-cell dysfunction and the incidence of type 2 diabetes in humans (Bugliani *et al*, 2013). Here, we show secretagogin mRNA levels to closely correlate with ubiquitin carboxyl-terminal hydrolase USP9X expression in humans. In experimental models, Ca^{2+}-bound secretagogin interacts with both USP9X and USP7, promoting their deubiquitinating activity. Notably, USP7 and USP9X chiefly control the levels of proteins determining cell cycle progression and apoptosis (e.g. p53, Mcl-1 PCNA, Chk1; Li *et al*, 2002; Yan *et al*, 2014; Kashiwaba *et al*, 2015; Lecona *et al*, 2016; McGarry *et al*, 2016). Consequently, the decreased enzymatic activity of ubiquitin carboxyl-terminal hydrolases results in increased ubiquitination and degradation of proteins essential for cell survival. These facts link secretagogin deficiency to β-cell apoptosis, particularly since acute inhibition of the proteasome is sufficient to recover β-cell viability upon silencing of secretagogin expression *in vitro*.

Pancreatic β- and α-cells express key enzymes for anandamide metabolism (Akiba *et al*, 2004; Malenczyk *et al*, 2013, 2015). Moreover, substantial levels of circulating anandamide are found in blood (Matias *et al*, 2006). Taking these data together, both autocrine and paracrine activation of TRPV1s present on β-cells could be hypothesized to regulate secretagogin expression. In fact, autocrine events or lateral ligand diffusion in β-cell membranes might be favoured when considering that anandamide uses an intracellular site to bind the TRPV1 receptor (van der Stelt *et al*, 2005). Notably, endocannabinoids and endovanilloids acting on TRP channels have been shown to regulate intracellular Ca^{2+} level (De Petrocellis *et al*, 2007), pancreas development (Malenczyk *et al*, 2015), β-cell turnover (Skrzypski *et al*, 2015) and insulin secretion (Akiba *et al*, 2004). Despite increased endocannabinoid levels, including anandamide, in obesity and diabetes (Matias *et al*, 2006; Starowicz *et al*, 2008), secretagogin expression in these conditions is downregulated (Hasegawa *et al*, 2013). As shown in *Trpv1*$^{-/-}$ mice, chronically increased anandamide levels can lead to desensitization and/or intracellular delocalization and degradation of TRPV1s (Rossi *et al*, 2011; Sanz-Salvador *et al*, 2012; Chen *et al*, 2015) and consequently disrupt secretagogin expression, thus priming β-cell death. Importantly, physiological concentrations of anandamide are expected to

serve as modulatory tonic stimuli for TRPV1-dependent Ca^{2+} influx and promote *"on-demand"* expression. It is noteworthy that *Trpv1*$^{-/-}$ mice have been shown to preserve healthy glucose metabolism (Riera *et al*, 2014) unless subjected to high fat diet (Lee *et al*, 2015). We found that the number of pancreatic islet in *Trpv1*$^{-/-}$ mice is unchanged compared to their wild-type littermates (data not shown). Yet, as we previously showed, the average size of islet in *Trpv1*$^{-/-}$ mice is increased due to a higher β-cell number (Malenczyk *et al*, 2015). These changes could be seen as compensatory to the chronic reduction of secretagogin levels in *Trpv1*$^{-/-}$ β-cells. Thus, the results presented here also provide an alternative and equally beneficial secondary target for capsaicin patches clinically indicated for pain relief associated with diabetic neuropathy.

Undoubtedly, Ca^{2+} influx in β-cells does not exclusively depend on the activity of TRPVs. Instead, the activity of other receptors and channels such as TRPCs (Qian *et al*, 2002), TRPMs (Cheng *et al*, 2007), NMDA receptors (Inagaki *et al*, 1995) and M$_3$ muscarinic receptors (Molina *et al*, 2014) that move Ca^{2+} across the plasmalemma, likely jointly regulates secretagogin expression. Glucose metabolism-dependent activity of voltage-gated L-, P/Q- and T-type Ca^{2+} channels is considered the primary factor affecting Ca^{2+} homoeostasis in pancreatic β-cells (Braun *et al*, 2008). Interestingly, a physiological glucose concentration (~5 mM) has been shown to most significantly, yet moderately stimulate the activity of the secretagogin promoter in insulinoma cells (Skovhus *et al*, 2006). This finding, particularly considering essential ramifications of the continued presence of secretagogin in β-cells is compatible with a *persistent* demand on secretagogin expression. Thus, if one places secretagogin as a "master regulator" of β-cell function and survival, then manifold signalling pathways likely converge on this Ca^{2+}-sensor to maintain its steady-state levels, particularly under pathophysiological conditions of hypo- or hyperglycaemia. The concept that the expressional upregulation of secretagogin transcription is sensitive to rapid and phasic elevations in intracellular Ca^{2+} is supported by the finding that KCl inhibits, while any Ca^{2+}-permeable receptor we tested augments this regulatory step. Therefore, we view secretagogin as a key intracellular regulator that can respond to regionalized and transient Ca^{2+} elevation, which arises upon glucose-independent signalling events to superposition onto glucose metabolism-driven signal transduction cascades. Overall, our findings of a TRPV1-to-secretagogin signalling axis in genetic models and humans offers a novel and tangible therapeutic target for restoring β-cell mass and function in diabetes.

Materials and Methods

Cell lines

INS-1E cells (Merglen *et al*, 2004) were cultured at 37°C in RPMI-1640 medium supplemented with glutamine (2 mM), glucose (11 mM), HEPES (10 mM), heat-inactivated foetal bovine serum (FBS; 5%), sodium pyruvate (1 mM), β-mercaptoethanol (50 μM), penicillin (50 μg/ml) and streptomycin (100 μg/ml). Cells were routinely sub-cultured in 24-well plates up to passage 120, and allowed to reach ~80% confluence. Knock-down of secretagogin expression was achieved by the co-application of secretagogin siRNA (50 nM; Santa Cruz) and jetPRIME transfection reagent

(polyplus-transfection SA) for 48 h. Scrambled siRNA (50 nM, Santa Cruz) was used as control. Ca^{2+}-free conditions were established by addition of EGTA (1 mM) to modified Krebs-Ringer bicarbonate HEPES buffer containing (in mM): 135 NaCl, 3.6 KCl, 0.5 $MgCl_2$, 1.5 NaH_2PO_4, 5 $NaHCO_3$, 10 HEPES at pH 7.4.

Generation of secretagogin$^{-/-}$ and β-$Scgn^{CKO}$ mice

Secretagogin$^{-/-}$ ($Scgn^{-/-}$) mice (Hanics et al, 2017) were custom-generated at MMRRC (University of California, Davis, Mouse Biology Program) using the "two-in-one" targeting strategy (Skarnes et al, 2011), which generates full knock-outs by expressing a termination signal after exon 3 of the secretagogin gene. The ensuing truncated protein terminates before the first EF-hand domain, excluding Ca^{2+}-binding activity. To generate β-cell-specific secretagogin knock-out mice (β-$Scgn^{CKO}$), $Scgn^{floxed/floxed}$ mice were bred with *Ins1*-Cre^{ERT} mice (Jackson #024709). β-$Scgn^{CKO}$ and wild-type mice (4-week old) were intraperitoneally injected with tamoxifen daily over a period of 5 days (200 mg/kg b.w. freshly dissolved in corn oil, both from Sigma; Tamarina et al, 2014). Secretagogin deletion was confirmed a week after the last tamoxifen injection (Fig EV4F–H). Animals (including *Trpv1*$^{-/-}$ mice, Jackson #3770) were kept under standard housing conditions with a 12-h/12-h light/dark cycle and food and water available *ad libitum*. Experiments on live animals conformed to the European Communities Council Directive (86/609/EEC) were approved by regional ethical committees and regulated by applicable local laws (Tierversuchsgesetz 2012, BGBI, Nr. 114/2012, Austria). Particular effort was directed towards minimizing the number of animals used and their suffering during experiments.

Isolation of pancreatic islets

Islets of wild-type and secretagogin$^{-/-}$ mice were obtained after perfusion of their pancreata with Hank's balanced salt solution (HBSS; Invitrogen/Gibco) containing collagenase (type I, 0.33 mg/ml; Sigma) and HEPES (25 mM) followed by purification on Histopaque 1077 gradients (Sigma). After repeated washes in HBSS containing 10% FBS, isolated islets were maintained in RPMI-1640 medium supplemented as above in humidified atmosphere (5% CO_2) at 37°C overnight prior to the commencement of hormone release measurements, assessment of gene expression or protein levels.

Calcium imaging

Single cells were prepared by isolation of pancreatic islets using the papain dissociation system (Worthington) with some modifications: 300 islets were incubated in 500 μl papain solution in EBSS supplemented with 0.005% DNase at 37°C for 20 min. Then, single cells were plated on 12-mm coverslips coated with matrigel (Corning) in complete RPMI-1640 (1:2 v/v ratio) and subsequently cultured in RPMI-1640 medium supplemented as above in humidified atmosphere (5% CO_2) at 37°C. Twenty-four hours later, Ca^{2+} responses from isolated pancreatic cells were recorded using the Ca^{2+} indicator Fura-2AM (Invitrogen). Ratiometric imaging was performed by using a VisiChrome monochromator (Visitron Systems) and Cool-Snap HQ^2 back-cooled camera (Photometrics) mounted onto a Zeiss Axiovert microscope equipped with a water-immersion 40×/differential interference contrast objective (Plan-Apochromat/N.A.

1.0). Ca^{2+} responses were recorded in the VisiView software (Visitron Systems) and statistically analysed in SigmaPlot 13.0 (Systat Software Inc.). Krebs-Ringer solution with low glucose was chosen as basic external solution and contained (in mM): 119 NaCl, 2.5 KCl, 1 NaH_2PO_4, 1.5 $CaCl_2$ and 1.5 $MgCl_2$, 20 HEPES, 3 glucose (pH 7.4). Experiments were performed at 25°C.

Molecular pharmacology

The effect of the following drugs, alone or in combination, on the subcellular localization and/or protein levels of Sp1, secretagogin, ubiquitinated proteins, apoptotic (e.g. cleaved caspase 3), proliferation (e.g. Ki67) and cell cycle (e.g. p53) markers as well as insulin secretion in INS-1E cells or pancreatic islets was assessed: 2-aminoethoxydiphenylborane (2-APB; non-selective TRPV3 agonist, 25 μM), (E)-N-[(4-hydroxy-3-methoxyphenyl) methyl]-8-methyl-6-nonenamide (capsaicin; TRPV1 agonist, 300 nM), N-[2-(4-chlorophenyl)ethyl]-1,3,4,5-tetrahydro-7,8-dihydroxy-2H-2-benzazepine-2-carbothioamide capsazepine; TRPV1 antagonist, 10 μM), 3,4-dihydro-N-(5-methyl-3-isoxazolyl)-α-phenyl-1(2H)-quinolineacetamide (CIM 0126; TRPM3 agonist, 1 μM), (2R,3S,4R)-3-hydroxy-2-[(1S)-1-hydroxy-2-methylpropyl]-4-methyl-5-oxo-2-pyrrolidinecarboxy-N-acetyl-L-cysteine thioester (lactacystin; proteasome inhibitor, 5 μM), N-[(phenylmethoxy)carbonyl]-L-leucyl-N-[(1S)-1-formyl-3-methylbutyl]-L-leucinamide (MG132; proteasome inhibitor, 5 μM) and N-methyl-D-aspartate (NMDA; NMDA receptor agonist 20 μM).

Production and purification of His$_6$-human secretagogin

Expression constructs for human secretagogin (UniProt ID: O76038) included amino acids 1–276. The coding sequence was amplified by PCR using appropriate primers, *Pfu*-Turbo polymerase (Stratagene) and cDNA as template and cloned by a ligation independent method into a pNIC28Bsa4 expression vector (GenBank accession no. EF198106) providing a cleavable N-terminal His$_6$-tag (H_2N-MHHHHHHSSGVDLGTENLYFQ*S). Protein was expressed in *E. coli* BL21 (DE3) at 21°C in Luria–Bertani broth (LB) supplemented with 30 μg/ml kanamycin. Protein expression was induced by the addition of 0.1 mM isopropyl β-D-1-thiogalactopyranoside at OD_{600} of 0.5–0.6. Cells were harvested 20 h post-induction, washed in 0.3 M NaCl and 10 mM Tris–HCl (pH 8.0) and disrupted by lysozyme (40 μg/ml) and DNaseI (2 μg/ml) treatment followed by sonication. Recombinant His$_6$-hSGCN was purified by affinity chromatography using His-Pur™ Ni-NTA resin (Thermo Scientific) and eluted with an increasing imidazole gradient. Using a desalting column (HiPrep-26/10; Pharmacia Biotech), the elution buffer was exchanged to 0.15 M NaCl and 25 mM Tris–HCl (pH 8.0). Size exclusion chromatography was then performed (Fig EV2A and C) on a Superdex-200 column (Pharmacia Biotech) equilibrated with 0.15 M NaCl and 25 mM Tris–HCl (pH 8.0). Pure protein samples were concentrated using a Centriprep YM-10 centrifugal device (Millipore) to 21.2 mg/ml. Protein concentration was determined according to Bradford using Pierce-Thermo reagents and bovine serum albumin (BSA) as standard. Samples were analysed by SDS–polyacrylamide gel electrophoresis, ESI-MS mass spectrometry and their folding integrity was confirmed by circular dichroism spectroscopy (Fig EV2B). Protein samples were aliquoted in a buffer containing 0.15 M NaCl

and 25 mM Tris–HCl (pH 8.0), flash-frozen in liquid N_2 and stored at −80°C.

In silico transcription factor binding site prediction and firefly luciferase assay

A 1,400-bp fragment (−1,400 to +1) of the 5′ flanking region of both the murine (NC_000079.6) and human (NC_000006.12) secretagogin genes was analysed for potential transcription factor binding sites using the open-label PROMO software (http://alggen.lsi.upc.es/cgi-bin/promo_v3/promo/promoinit.cgi?dirDB = TF_6.4). For activity determination of the murine secretagogin promoter, its 1,400-bp 5′ flanking region (−1,400 to +1) referred to as full *Scgn* promoter or a deletion mutant lacking predicted Sp1 binding sites at bps −548 to −542, −485 to −480 and −11 to −3 (Fig 2C) were custom-synthesized (Eurofins Genomics) by cloning between *XhoI* and *NcoI* restriction sites into a pGL3-Basic vector (Promega) also containing a firefly luciferase cassette. Subsequently, INS-1E cells cultured in 96-well plates (50,000/well) were co-transfected with either construct and a pCMV-green *Renilla* luciferase vector (Thermo Fisher; as control) using jetPRIME transfection reagent (Polyplus-transfection SA). Eighteen h later, cells were stimulated with capsaicin (300 nM) for 30 min. After an additional 3.5 h, firefly and *Renilla* luciferase lumiensence was measured using the Dual-Luciferase® Reporter Assay System (Promega) on a GloMax® luminometer (Promega). Data were analysed as a ratio of firefly to *Renilla* luciferase lumiensence intensity and normalized to values from unstimulated control cells.

RNA isolation and gene expression analysis

Total RNA from INS-1E cells and pancreatic islets was isolated using the RNeasy Mini Kit (Qiagen) followed by DNase digestion and verifying RNA integrity on 2% agarose gels (500 ng RNA). cDNA was prepared by reverse transcription with random primers using the High-capacity cDNA Reverse Transcription Kit (Applied Biosystems). PCR was performed using 2× Master mix (Promega) and specific primer pairs (Table EV4). PCR products were resolved on 2% agarose gels and imaged on a ChemiDoc XRS$^+$ system (Bio-Rad). Quantitative PCR analysis (CFX Connect, Bio-Rad) was performed using 50 ng of cDNA template, iTaq Universal SYBR Green Supermix (Bio-Rad) and specific primer pairs (Table EV4).

Western blotting

Proteins were extracted from INS-1E cells or isolated pancreatic islets using a radioimmunoprecipitation assay buffer containing (in mM): 50 Tris (pH 7.4), 150 NaCl, 10 NaF, 5 EDTA (pH 8.0), 1 Na_3VO_4, 1 PMSF, 1% TX-100, pepstatin A (5 μg/μl), leupeptin (10 μg/μl) and aprotinine (2 μg/μl), optionally supplemented with MG132 (Tocris; 10 μM; to inhibit protein deubiquitination). Protein lysates were centrifuged at 12,000 *g* at 4°C for 10 min. For the analysis of total protein levels, lysates were pre-incubated with carbocyanine (Cy) 5 labelling buffer (GE Healthcare) for 10 min. Samples were denatured in loading buffer (GE Healthcare) and boiled at 95°C for 5 min. Proteins were probed by loading 20 μg aliquots under denaturing conditions on SDS–PAGE (13.5% or 8–18% gradient gels), followed by wet transfer onto PVDF membranes. Primary

antibodies were listed in Table EV5. After exposure to Cy3- or Cy5-conjugated secondary antibodies (GE Healthcare, 1:2,500; 1 h), target proteins were visualized using an automated Amersham WB system (GE Healthcare).

Tissue preparation, immunocytochemistry and immunohistochemistry

For immunocytochemistry, cells were plated on 12-mm coverslips coated with poly-D-lysine (0.001%), washed in 0.1 M phosphate buffer (PB, pH 7.4) and immersion fixed in 4% paraformaldehyde (PFA) for 20 min. Mice were transcardially perfused with ice-cold 0.1 M PB, followed by 4% PFA in PB (100 ml at 3 ml/min flow speed). Pancreata were rapidly dissected and post-fixed in 4% PFA overnight. After equilibrating in 30% sucrose for 48–72 h, tissues were cryosectioned at a thickness of 14 μm (Leica CM1850) and thaw-mounted onto SuperFrost$^+$ glass slides. After rinsing in 0.1 M PB, specimens were exposed to a blocking solution composed of 0.1 M PB, 10% normal donkey serum, 5% BSA and 0.3% TX-100 for 3 h followed by overnight incubation with select combinations of primary antibodies (Table EV5). Cy2, 3 or 5-conjugated secondary antibodies (1:300, Jackson) were applied in 0.1 M PB supplemented with 2% BSA (20–22°C, 2 h). Nuclei were routinely counterstained with Hoechst 33342 (1:20,000; Sigma). Cells and pancreas sections were imaged on a Zeiss LSM880 laser-scanning microscope equipped with a Plan-Apochromat 40×/1.3 oil immersion objective at 1.0–2.5× optical zoom. Images were acquired in the ZEN2010 software package. Quantitative analysis was performed using ImageJ 1.45 with appropriate plug-ins. Multipanel images were assembled in CorelDraw X7 (Corel Corp.).

Electron microscopy

Male mice (*n* = 3/group) were fasted overnight (~15 h) with water available *ad libitum.* Thirty min after intraperitoneal glucose challenge (2 g/kg body weight), mice were euthanized by cervical dislocation and transcardially perfused with 0.9% NaCl, followed by fixative (4% PFA, 0.1% glutaraldehyde, 15% picric acid) in PB (3 ml/min flow speed). Pancreata were then dissected out and post-fixed overnight in the same fixative. After vigorous washing in ice-cold PB, vibratome sections were cut (40–60 μm) containing pancreatic islets. Sections were repeatedly washed in PB, cryoprotected in 30% sucrose and subsequently freeze–thawed three times in liquid N_2. After extensive washing in PB, slices were incubated with H_2O_2 (1%, 20–22°C, 20 min) to block endogenous peroxidase activity. After washing again with PB, sections were incubated with rabbit anti-insulin antibody (1:400; 4°C, 48 h). Sections were extensively washed, incubated with biotinylated horse anti-mouse secondary antibody (1:250; Vector Labs., 20–22°C, 2 h), rinsed again and then exposed to pre-formed avidin biotin-peroxidase complexes (1:200; Vector, 2 h) and developed with 3,3′-diaminobenzidine (5 mg/ml, 0.03% H_2O_2 as substrate). Sections were then osmificated (1% OsO_4 in PB, 15 min), dehydrated in increasing ethanol concentrations followed by flat embedding in Durcupan (FLUKA, ACM). Ultrathin sections (60 nm) were cut on a Leica ultramicrotome, collected on Formvar-coated single-slot grids, and analysed with a Tecnai 10 electron microscope (FEI). Investigators were blinded to the experimental groups during the entire

procedure. Quantitative analysis ($n = 30$ cells/group) was performed using ImageJ 1.45 with appropriate plug-ins. The total number of insulin-containing secretory vesicles was normalized to the cytoplasm surface. Insulin granules directly contacting the plasmalemma (Fig EV5E′ and E$_1$′) were considered as docked, and their number was normalized to the length of the plasma membrane (expressed as vesicle/μm).

Pull-down assay

Sixty micro gram of His$_6$-tagged secretagogin and INS-1E cell lysate (400 μg of protein) was mixed in binding buffer (pH 7.4) containing (in mM): 25 Tris–HCl, 300 NaCl, 0.1 CaCl$_2$, 10 imidazole to obtain a 100-μl total sample volume, and incubated together with 40 μl of pre-equilibrated Ni-NTA beads in Spin-X Centrifuge Tube Filter 0.22 μm cellulose acetate columns (Costar) at 20–22°C for 30 min. In control experiments, His$_6$-tagged secretagogin was replaced with binding buffer alone to obtain 100 μl of total sample. Flow-through fractions were removed after spinning at 1,500 g for 30 s. Beads were washed (3×) with 100 μl buffer (in mM): 25 Tris–HCl, 300 NaCl, 0.1 CaCl$_2$, 50 imidazole. Proteins were eluted with 70 μl elution buffer composed of (in mM): 25 Tris–HCl, 300 NaCl, 0.1 CaCl$_2$ and 300 imidazole. Samples were stored at −80°C until processing for mass spectrometry.

LC-MS/MS analysis of protein complexes including statistics

Eluted proteins (17.5 μg) of His$_6$-secretagogin ($n = 3$) and control pull-downs ($n = 3$) were digested with trypsin via filter-aided sample preparation (Wisniewski *et al*, 2009) with minor modifications (Aradska *et al*, 2015). Tryptic digests were desalted and concentrated on customized reversed-phase C18 stage tips (Rappsilber *et al*, 2007). Purified peptides were reconstituted in 5% formic acid (FA), and 2 × 1 μg of each sample (technical replicates) was analysed by liquid chromatography-tandem mass spectrometry (LC-MS/MS). Peptides were separated on an Ultimate 3000 nanoRSLC system (Thermo Fisher) equipped with a PM100-C18 precolumn (3 μm, 75 μm × 20 mm) and a PepMap-C18 analytical column (2 μm, 75 μm × 500 mm). Ten μl of each sample was loaded onto the trap column for 5 min using 0.1% FA in water at a flow rate of 5 μl/min. Afterwards, peptides were forward-flushed to and separated on the analytical column at a flow rate of 300 nl/min using a 55-min gradient ranging from 5 to 37.5% solvent B, followed by a 5-min gradient from 37.5 to 50% solvent B and finally, to 90% solvent B for 5 min before re-equilibration to 5% solvent B (solvent A: 0.1% FA in water; solvent B: 0.1% FA in 80% acetonitrile). Eluted peptides were in-line analysed on a Thermo Q-Exactive Plus mass spectrometer (Thermo Fisher) in positive ion mode. MS scans were performed in a range of m/z 380–1,800 at a resolution of 70,000. In a data-dependent acquisition mode, the 20 most intense precursor ions were selected and fragmented via higher energy collisional dissociation at 27% normalized collision energy with a fixed first mass of 100 m/z. Fragment ions were detected at a resolution of 17,500. Dynamic exclusion of selected peptides was enabled for 60 s, and maximal accumulation times were set to 100 and 50 ms in MS and MS^n modes, respectively. To describe the secretagogin-specific interactome, all MS raw data files were analysed by the open-source software MaxQuant 1.5.3.30 (Cox

& Mann, 2008) as previously described (Smidak *et al*, 2016). Proteins were identified against the Swiss-Prot rat (*Rattus norvegicus*) reference proteome database (as of November 2015; 31,457 entries) permitting a mass tolerance of 5 ppm and 20 ppm for MS and MS^2 spectra, respectively. Maximum two missed cleavages were allowed and minimum two peptide identifications per protein were required. Carbamidomethylation of cysteines was set as fixed modification while methionine oxidation and N-terminal protein acetylation were chosen as variable modifications. For both peptide and protein identification, the false discovery rate (FDR) was set to 0.01. MaxQuant results were further processed using the Perseus statistical package (version 1.5.4.1) to identify interactors from label-free data (LFQ intensities). Proteins were filtered for reversed sequences, contaminants, and if they were only identified by site. Intensity values were log$_2$-transformed and proteins were further filtered for having LFQ values in minimum three samples at least in one group (either in the target or in the control). Zero intensities were input and replaced by normal distribution, and secretagogin pull-downs were compared to control samples via two-sided Student's t-test with $P < 0.05$ (applying permutation-based FDR for truncation). Proteins with a minimum twofold increase of their LFQ intensities in the target pull-down were considered as specific for secretagogin if they were identified by at least two unique peptides.

LC-MS/MS analysis of endocannabinoid contents

Extraction, purification and quantification of anandamide from the blood of embryos at embryonic day 18.5 followed published protocols (De Marchi *et al*, 2003; Matias *et al*, 2006). After lipid extraction and pre-purification on silica gel columns, anandamide levels from three animals were analysed by isotope dilution using liquid chromatography-atmospheric pressure chemical ionization-mass spectrometry (Shimadzu LCMS-2020).

Insulin secretion and total insulin content ELISA assay

Pancreatic islets were incubated in drug-free modified Krebs-Ringer bicarbonate HEPES buffer (KRBHB) containing (in mM): 135 NaCl, 3.6 KCl, 1.5 CaCl$_2$, 0.5 MgCl$_2$, 1.5 NaH$_2$PO$_4$, 5 NaHCO$_3$, 10 HEPES (pH 7.4) and BSA (0.1%) supplemented with 2.75 mM glucose for 1 h. Subsequently, samples were transferred to microcentrifuge tubes at a density of 10 islets/tube. Islets were incubated in modified KRBHB supplemented with 2.75 mM glucose with or without 30 mM KCl or 16.5 mM glucose for 30 min. Alternatively, after overnight culturing, islets (30 islets/group) were homogenized in water using 27G needles. Homogenates were mixed with 0.18 M HCl in 96% EtOH (1:3 v/v ratio), incubated at 4°C for 16 h and centrifuged at 1,500 g at 4°C for 15 min. Supernatants were stored at −80°C until processing. Insulin levels were measured by a rat/mouse insulin ELISA Kit (Millipore) with insulin concentrations normalized to either the number of islets or β-cells.

Glucose tolerance test

Male mice ($n = 6$/group) were fasted overnight (~15 h) with water available *ad libitum*. Blood glucose level was measured from tail blood using a FreeStyle Lite glucose meter (Abbott Diabetes Care) before (baseline, 0 min) as well as 15, 30, 60, 90 and 120 min after

RNA-seq and histochemistry-based body-wide mapping of secretagogin distribution

Secretagogin expression in nervous and peripheral tissue in both human and mouse was determined based on (i) open-source RNA-seq data and (ii) cap analysis of gene expression (CAGE). RNA-seq data in human was directly imported from the Genotype-Tissue Expression Portal (GTEx; GTEx Consortium *et al*, 2013) while mouse RNA-seq data were obtained from the ENCODE project repository (Kundaje *et al*, 2015; Fig EV1A, Table EV6). Secretagogin transcription start sides were quantified based on FANTOM CAGE data (Carninci *et al*, 2005) using the ZENBU genome browser (http://fantom.gsc.riken.jp/zenbu/). Antibody-based protein distribution maps in human and mouse tissues were extracted from the Human Protein Atlas project (www.proteinatlas.org) based on antibodies raised against the C-terminal domain of secretagogin complemented by immunohistochemistry of particular tissues (Fig EV1B, Table EV6) using the same antibody (Mulder *et al*, 2010).

Gene expression in human subjects

Islets from 202 cadaver donors of European ancestry were provided by the Nordic Islet Transplantation Programme (http://www.nordicislets.org). All procedures were approved by the ethics committee at Lund University and performed as previously described (Fadista *et al*, 2014). Briefly, purity of islets was assessed by dithizone followed by islets culture in CMRL 1066 (ICN Biomedicals) supplemented with 10 mM HEPES, 2 mM L-glutamine, 50 μg/ml gentamicin, 0.25 μg/ml Fungizone (GIBCO), 20 μg/ml ciprofloxacin (Bayer Healthcare) and 10 mM nicotinamide at 37°C (5% CO_2) for 1–9 days prior to RNA preparation. Total RNA was isolated with the AllPrep DNA/RNA Mini Kit following the manufacturer's instructions (Qiagen). RNA quality and concentration were measured using an Agilent 2100 bioanalyzer (Bio-Rad) and a Nanodrop ND-1000 (NanoDrop Technologies). Samples were stratified based upon glucose tolerance estimated from HbA1c, that is donors with normal glucose tolerance (HbA1c < 6%, $n = 123$), impaired glucose tolerance (IGT, 6% ≤ HbA1c < 6.5%, $n = 47$), and type 2 diabetes (HbA1c ≥ 6.5%, $n = 32$). A linear model adjusting for age and sex as implemented in the R Matrix eQTL package was used to determine the expression of genes associated with glucose tolerance status. Raw data were base called and de-multiplexed using CASAVA 1.8.2 (Illumina) before alignment to hg19 with STAR. To count the number of reads aligned to specific transcripts feature Counts (v 1.4.4, http://bioinf.wehi.edu.au/featureCounts/) was used. Raw data were normalized using trimmed mean of M-values (TMM) and transformed into $\log_2$ counts per million ($\log_2$CPM) using voom (limma R, Bioconductor) before linear modelling. After TMM-normalization, batch effects were removed using the Combat function (sva package).

Single-cell RNA-seq of pancreatic islets

Analysis was performed based on a publicly available expression matrix (Segerstolpe *et al*, 2016) from 270 human β-cells from six

healthy ($n = 171$ cells) and four type 2 diabetic donors ($n = 99$ cells). Briefly, human tissue and primary islets were purchased from Prodo Laboratories Inc., providing islets isolated from donor pancreata obtained from deceased individuals with research consent from Organ Procurement Organizations. Human islet samples (85–95% pure) were cultured for 4 days in complete Prodo Islet Media Standard PIM(S) after arrival. Islets were dissociated and distributed by FACS into 384-well plates. Single-cell RNA-seq libraries were produced with the Smart-seq2 protocol (Segerstolpe *et al*, 2016). Sequencing was carried out on an Illumina HiSeq 2000 generating 43-bp single-end reads. Sequence reads were aligned towards the human genome (hg19 assembly) using STAR (v2.3.0e), and uniquely aligned reads within RefSeq gene annotations were used to quantify gene expression as RPKMs using the "rpkmforgenes" routine (sandberg.cmb.ki.se/media/data/rnaseq/).

Statistics

All experiments were performed in triplicate unless stated otherwise. Data from pharmacology experiments were analysed using one-way ANOVA followed by pairwise comparisons where appropriate. Student's *t*-test (independent group design) was used to statistically evaluate data on pancreatic islet morphology, INS-1E proliferation and apoptosis and gene expression. Data from Ca^{2+}-imaging and RNA-seq were analysed using the Mann–Whitney rank-sum test. Data are expressed as means ± s.d. unless specified. Fold changes represent the percentage change from the untreated (control) value in individual experiments. A $P < 0.05$ value was considered statistically significant.

Accession numbers

Raw data on single-cell RNA-seq of pancreatic beta cells and human islets sequenced in bulk were deposited in ArrayExpress (E-MTAB-5061) and Gene Expression Omnibus (GSE50398), respectively. The mass spectrometry proteomics data have been deposited to the ProteomeXchange Consortium via the PRIDE partner repository with the data set identifier PXD006544.

Expanded View for this article is available online.

and databases; KM and THa wrote the manuscript, which was proofread and approved by all authors.

Conflict of interest

References

Akiba Y, Kato S, Katsube K, Nakamura M, Takeuchi K, Ishii H, Hibi T (2004) Transient receptor potential vanilloid subfamily 1 expressed in pancreatic islet beta cells modulates insulin secretion in rats. *Biochem Biophys Res Commun* 321: 219−225

Allen JR, Nguyen LX, Sargent KE, Lipson KL, Hackett A, Urano F (2004) High ER stress in beta-cells stimulates intracellular degradation of misfolded insulin. *Biochem Biophys Res Commun* 324: 166−170

Alpar A, Attems J, Mulder J, Hokfelt T, Harkany T (2012) The renaissance of Ca^{2+}-binding proteins in the nervous system: secretagogin takes center stage. *Cell Signal* 24: 378−387

Aradska J, Bulat T, Sialana FJ, Birner-Gruenberger R, Erich B, Lubec G (2015) Gel-free mass spectrometry analysis of *Drosophila* melanogaster heads. *Proteomics* 15: 3356−3360

Araki E, Oyadomari S, Mori M (2003) Impact of endoplasmic reticulum stress pathway on pancreatic beta-cells and diabetes mellitus. *Exp Biol Med (Maywood)* 228: 1213−1217

Ardestani A, Paroni F, Azizi Z, Kaur S, Khobragade V, Yuan T, Frogne T, Tao W, Oberholzer J, Pattou F, Kerr CJ, Maedler K (2014) MST1 is a key regulator of beta cell apoptosis and dysfunction in diabetes. *Nat Med* 20: 385−397

Bauer MC, O'Connell DJ, Maj M, Wagner L, Cahill DJ, Linse S (2011) Identification of a high-affinity network of secretagogin-binding proteins involved in vesicle secretion. *Mol BioSyst* 7: 2196−2204

Bazwinsky-Wutschke I, Wolgast S, Muhlbauer E, Peschke E (2010) Distribution patterns of calcium-binding proteins in pancreatic tissue of non-diabetic as well as type 2 diabetic rats and in rat insulinoma beta-cells (INS-1). *Histochem Cell Biol* 134: 115−127

Birkenkamp-Demtroder K, Wagner L, Brandt SF, Bording AL, Gartner W, Scherubl H, Heine B, Christiansen P, Orntoft TF (2005) Secretagogin is a novel marker for neuroendocrine differentiation. *Neuroendocrinology* 82: 121−138

Bitto E, Bingman CA, Bittova L, Frederick RO, Fox BG, Phillips GN Jr (2009) X-ray structure of Danio rerio secretagogin: a hexa-EF-hand calcium sensor. *Proteins* 76: 477−483

Bollo M, Paredes RM, Holstein D, Zheleznova N, Camacho P, Lechleiter JD (2010) Calcineurin interacts with PERK and dephosphorylates calnexin to relieve ER stress in mammals and frogs. *PLoS ONE* 5: e11925

Braun M, Ramracheya R, Bengtsson M, Zhang Q, Karanauskaite J, Partridge C, Johnson PR, Rorsman P (2008) Voltage-gated ion channels in human pancreatic beta-cells: electrophysiological characterization and role in insulin secretion. *Diabetes* 57: 1618−1628

Bugliani M, Liechti R, Cheon H, Suleiman M, Marselli L, Kirkpatrick C, Filipponi F, Boggi U, Xenarios I, Syed F, Ladriere L, Wollheim C, Lee MS, Marchetti P (2013) Microarray analysis of isolated human islet transcriptome in type 2 diabetes and the role of the ubiquitin-proteasome system in pancreatic beta cell dysfunction. *Mol Cell Endocrinol* 367: 1−10

Butler AE, Janson J, Bonner-Weir S, Ritzel R, Rizza RA, Butler PC (2003) Beta-cell deficit and increased beta-cell apoptosis in humans with type 2 diabetes. *Diabetes* 52: 102−110

Carninci P, Kasukawa T, Katayama S, Gough J, Frith MC, Maeda N, Oyama R, Ravasi T, Lenhard B, Wells C, Kodzius R, Shimokawa K, Bajic VB, Brenner SE, Batalov S, Forrest AR, Zavolan M, Davis MJ, Wilming LG, Aidinis V, *et al* (2005) The transcriptional landscape of the mammalian genome. *Science* 309: 1559−1563

Celio MR (1990) Calbindin-D-28k and parvalbumin in the rat nervous system. *Neuroscience* 35: 375−475

Chen J, Li L, Li Y, Liang X, Sun Q, Yu H, Zhong J, Ni Y, Chen J, Zhao Z, Gao P, Wang B, Liu D, Zhu Z, Yan Z (2015) Activation of TRPV1 channel by dietary capsaicin improves visceral fat remodeling through connexin43-mediated Ca^{2+} influx. *Cardiovasc Diabetol* 14: 22

Cheng H, Beck A, Launay P, Gross SA, Stokes AJ, Kinet JP, Fleig A, Penner R (2007) TRPM4 controls insulin secretion in pancreatic beta-cells. *Cell Calcium* 41: 51−61

Clapham DE, Runnels LW, Strubing C (2001) The TRP ion channel family. *Nat Rev Neurosci* 2: 387−396

Cox J, Mann M (2008) MaxQuant enables high peptide identification rates, individualized p.p.b.-range mass accuracies and proteome-wide protein quantification. *Nat Biotechnol* 26: 1367−1372

Creutz CE, Liou A, Snyder SL, Brownawell A, Willison K (1994) Identification of the major chromaffin granule-binding protein, chromobindin A, as the cytosolic chaperonin CCT (chaperonin containing TCP-1). *J Biol Chem* 269: 32035−32038

De Marchi N, De Petrocellis L, Orlando P, Daniele F, Fezza F, Di Marzo V (2003) Endocannabinoid signalling in the blood of patients with schizophrenia. *Lipids Health Dis* 2: 5

De Petrocellis L, Marini P, Matias I, Moriello AS, Starowicz K, Cristino L, Nigam S, Di Marzo V (2007) Mechanisms for the coupling of cannabinoid receptors to intracellular calcium mobilization in rat insulinoma beta-cells. *Exp Cell Res* 313: 2993−3004

Dekker C, Stirling PC, McCormack EA, Filmore H, Paul A, Brost RL, Costanzo M, Boone C, Leroux MR, Willison KR (2008) The interaction network of the chaperonin CCT. *EMBO J* 27: 1827−1839

Deng S, Vatamaniuk M, Huang X, Doliba N, Lian MM, Frank A, Velidedeoglu E, Desai NM, Koeberlein B, Wolf B, Barker CF, Naji A, Matschinsky FM, Markmann JF (2004) Structural and functional abnormalities in the islets isolated from type 2 diabetic subjects. *Diabetes* 53: 624−632

van Der Luit AH, Olivari C, Haley A, Knight MR, Trewavas AJ (1999) Distinct calcium signaling pathways regulate calmodulin gene expression in tobacco. *Plant Physiol* 121: 705−714

Di Marzo V, De Petrocellis L (2012) Why do cannabinoid receptors have more than one endogenous ligand? *Philos Trans R Soc Lond B Biol Sci* 367: 3216−3228

Ericsson UB, Hallberg BM, Detitta GT, Dekker N, Nordlund P (2006) Thermofluor-based high-throughput stability optimization of proteins for structural studies. *Anal Biochem* 357: 289−298

Fadista J, Vikman P, Laakso EO, Mollet IG, Esguerra JL, Taneera J, Storm P, Osmark P, Ladenvall C, Prasad RB, Hansson KB, Finotello F, Uvebrant K, Ofori JK, Di Camillo B, Krus U, Cilio CM, Hansson O, Eliasson L, Rosengren AH, *et al* (2014) Global genomic and transcriptomic analysis of human pancreatic islets reveals novel genes influencing glucose metabolism. *Proc Natl Acad Sci USA* 111: 13924−13929

Gao H, Miyata K, Bhaskaran MD, Derbenev AV, Zsombok A (2012) Transient receptor potential vanilloid type 1-dependent regulation of liver-related

neurons in the paraventricular nucleus of the hypothalamus diminished in the type 1 diabetic mouse. *Diabetes* 61: 1381−1390

German MS, Moss LG, Rutter WJ (1990) Regulation of insulin gene expression by glucose and calcium in transfected primary islet cultures. *J Biol Chem* 265: 22063−22066

Glotzer M, Murray AW, Kirschner MW (1991) Cyclin is degraded by the ubiquitin pathway. *Nature* 349: 132−138

Goodyer WR, Gu X, Liu Y, Bottino R, Crabtree GR, Kim SK (2012) Neonatal beta cell development in mice and humans is regulated by calcineurin/NFAT. *Dev Cell* 23: 21−34

Grantham J, Ruddock LW, Roobol A, Carden MJ (2002) Eukaryotic chaperonin containing T-complex polypeptide 1 interacts with filamentous actin and reduces the initial rate of actin polymerization *in vitro*. *Cell Stress Chaperones* 7: 235−242

GTEx Consortium, Lonsdale J, Thomas J, Salvatore M, Phillips R, Lo E, Shad S, Walters G, Walters G, Walters G, Foster B, Moser M, Karasik E, Gillard B, Ramsey K, Sullivan S, Bridge J, Magazine H, Syron J, Fleming J, *et al* (2013) The genotype-tissue expression (GTEx) project. *Nat Genet*, 45: 580−585

Hanics J, Szodorai E, Tortoriello G, Malenczyk K, Keimpema E, Lubec G, Hevesi Z, Lutz MI, Kozsurek M, Puskar Z, Toth ZE, Wagner L, Kovacs GG, Hokfelt TG, Harkany T, Alpar A (2017) Secretagogin-dependent matrix metalloprotease-2 release from neurons regulates neuroblast migration. *Proc Natl Acad Sci USA* 114: E2006−E2015

Harding HP, Zhang Y, Zeng H, Novoa I, Lu PD, Calfon M, Sadri N, Yun C, Popko B, Paules R, Stojdl DF, Bell JC, Hettmann T, Leiden JM, Ron D (2003) An integrated stress response regulates amino acid metabolism and resistance to oxidative stress. *Mol Cell* 11: 619−633

Hasegawa K, Wakino S, Kimoto M, Minakuchi H, Fujimura K, Hosoya K, Komatsu M, Kaneko Y, Kanda T, Tokuyama H, Hayashi K, Itoh H (2013) The hydrolase DDAH2 enhances pancreatic insulin secretion by transcriptional regulation of secretagogin through a Sirt1-dependent mechanism in mice. *FASEB J* 27: 2301−2315

Heit JJ, Apelqvist AA, Gu X, Winslow MM, Neilson JR, Crabtree GR, Kim SK (2006) Calcineurin/NFAT signalling regulates pancreatic beta-cell growth and function. *Nature* 443: 345−349

Held K, Kichko T, De CK, Klaassen H, Van BR, Vanherck JC, Marchand A, Reeh PW, Chaltin P, Voets T, Vriens J (2015) Activation of TRPM3 by a potent synthetic ligand reveals a role in peptide release. *Proc Natl Acad Sci USA* 112: E1363−E1372

Henquin JC, Ishiyama N, Nenquin M, Ravier MA, Jonas JC (2002) Signals and pools underlying biphasic insulin secretion. *Diabetes* 51(Suppl. 1): S60−S67

Henquin JC, Mourad NI, Nenquin M (2012) Disruption and stabilization of beta-cell actin microfilaments differently influence insulin secretion triggered by intracellular Ca^{2+} mobilization or store-operated Ca^{2+} entry. *FEBS Lett* 586: 89−95

Hu H, Grandl J, Bandell M, Petrus M, Patapoutian A (2009) Two amino acid residues determine 2-APB sensitivity of the ion channels TRPV3 and TRPV4. *Proc Natl Acad Sci USA* 106: 1626−1631

Inagaki N, Kuromi H, Gonoi T, Okamoto Y, Ishida H, Seino Y, Kaneko T, Iwanaga T, Seino S (1995) Expression and role of ionotropic glutamate receptors in pancreatic islet cells. *FASEB J* 9: 686−691

Ize-Ludlow D, Lightfoot YL, Parker M, Xue S, Wasserfall C, Haller MJ, Schatz D, Becker DJ, Atkinson MA, Mathews CE (2011) Progressive erosion of beta-cell function precedes the onset of hyperglycemia in the NOD mouse model of type 1 diabetes. *Diabetes* 60: 2086−2091

Kashiwaba S, Kanao R, Masuda Y, Kusumoto-Matsuo R, Hanaoka F, Masutani C (2015) USP7 is a suppressor of PCNA ubiquitination and oxidative-stress-induced mutagenesis in human cells. *Cell Rep* 13: 2072−2080

Koch HB, Zhang R, Verdoodt B, Bailey A, Zhang CD, Yates JR III, Menssen A, Hermeking H (2007) Large-scale identification of c-MYC-associated proteins using a combined TAP/MudPIT approach. *Cell Cycle* 6: 205−217

Kundaje A, Meuleman W, Ernst J, Bilenky M, Yen A, Heravi-Moussavi A, Kheradpour P, Zhang Z, Wang J, Ziller MJ, Amin V, Whitaker JW, Schultz MD, Ward LD, Sarkar A, Quon G, Sandstrom RS, Eaton ML, Wu YC, Pfenning AR, *et al* (2015) Integrative analysis of 111 reference human epigenomes. *Nature* 518: 317−330

Lai M, Lu B, Xing X, Xu E, Ren G, Huang Q (2006) Secretagogin, a novel neuroendocrine marker, has a distinct expression pattern from chromogranin A. *Virchows Arch* 449: 402−409

Lecona E, Rodriguez-Acebes S, Specks J, Lopez-Contreras AJ, Ruppen I, Murga M, Munoz J, Mendez J, Fernandez-Capetillo O (2016) USP7 is a SUMO deubiquitinase essential for DNA replication. *Nat Struct Mol Biol* 23: 270−277

Lee E, Jung DY, Kim JH, Patel PR, Hu X, Lee Y, Azuma Y, Wang HF, Tsitsilianos N, Shafiq U, Kwon JY, Lee HJ, Lee KW, Kim JK (2015) Transient receptor potential vanilloid type-1 channel regulates diet-induced obesity, insulin resistance, and leptin resistance. *FASEB J* 29: 3182−3192

Li M, Chen D, Shiloh A, Luo J, Nikolaev AY, Qin J, Gu W (2002) Deubiquitination of p53 by HAUSP is an important pathway for p53 stabilization. *Nature* 416: 648−653

Lievremont JP, Rizzuto R, Hendershot L, Meldolesi J (1997) BiP, a major chaperone protein of the endoplasmic reticulum lumen, plays a direct and important role in the storage of the rapidly exchanging pool of Ca^{2+}. *J Biol Chem* 272: 30873−30879

Lin YF, Lee YF, Liang PH (2012) Targeting beta-tubulin:CCT-beta complexes incurs Hsp90- and VCP-related protein degradation and induces ER stress-associated apoptosis by triggering capacitative Ca^{2+} entry, mitochondrial perturbation and caspase overactivation. *Cell Death Dis* 3: e434

Maj M, Gartner W, Ilhan A, Neziri D, Attems J, Wagner L (2010) Expression of TAU in insulin-secreting cells and its interaction with the calcium-binding protein secretagogin. *J Endocrinol* 205: 25−36

Malenczyk K, Jazurek M, Keimpema E, Silvestri C, Janikiewicz J, Mackie K, Di Marzo V, Redowicz MJ, Harkany T, Dobrzyn A (2013) CB1 cannabinoid receptors couple to focal adhesion kinase to control insulin release. *J Biol Chem* 288: 32685−32699

Malenczyk K, Keimpema E, Piscitelli F, Calvigioni D, Bjorklund P, Mackie K, Di Marzo V, Hokfelt TG, Dobrzyn A, Harkany T (2015) Fetal endocannabinoids orchestrate the organization of pancreatic islet microarchitecture. *Proc Natl Acad Sci USA* 112: E6185−E6194

Marquard J, Otter S, Welters A, Stirban A, Fischer A, Eglinger J, Herebian D, Kletke O, Klemen MS, Stozer A, Wnendt S, Piemonti L, Kohler M, Ferrer J, Thorens B, Schliess F, Rupnik MS, Heise T, Berggren PO, Klocker N, *et al* (2015) Characterization of pancreatic NMDA receptors as possible drug targets for diabetes treatment. *Nat Med* 21: 363−372

Matias I, Gonthier MP, Orlando P, Martiadis V, De Petrocellis L, Cervino C, Petrosino S, Hoareau L, Festy F, Pasquali R, Roche R, Maj M, Pagotto U, Monteleone P, Di Marzo V (2006) Regulation, function, and dysregulation of endocannabinoids in models of adipose and beta-pancreatic cells and in obesity and hyperglycemia. *J Clin Endocrinol Metab* 91: 3171−3180

Matsumoto M, Minami M, Takeda K, Sakao Y, Akira S (1996) Ectopic expression of CHOP (GADD153) induces apoptosis in M1 myeloblastic leukemia cells. *FEBS Lett* 395: 143−147

McGarry E, Gaboriau D, Rainey MD, Restuccia U, Bachi A, Santocanale C (2016) The deubiquitinase USP9X maintains DNA replication fork stability and DNA damage checkpoint responses by regulating CLASPIN during S-phase. *Cancer Res* 76: 2384−2393

Merglen A, Theander S, Rubi B, Chaffard G, Wollheim CB, Maechler P (2004) Glucose sensitivity and metabolism-secretion coupling studied during two-year continuous culture in INS-1E insulinoma cells. *Endocrinology* 145: 667–678

Molina J, Rodriguez-Diaz R, Fachado A, Jacques-Silva MC, Berggren PO, Caicedo A (2014) Control of insulin secretion by cholinergic signaling in the human pancreatic islet. *Diabetes* 63: 2714–2726

Moon DO, Kang CH, Kang SH, Choi YH, Hyun JW, Chang WY, Kang HK, Koh YS, Maeng YH, Kim YR, Kim GY (2012) Capsaicin sensitizes TRAIL-induced apoptosis through Sp1-mediated DR5 up-regulation: involvement of Ca($^{2+}$) influx. *Toxicol Appl Pharmacol* 259: 87–95

Mulder J, Spence L, Tortoriello G, Dinieri JA, Uhlen M, Shui B, Kotlikoff MI, Yanagawa Y, Aujard F, Hokfelt T, Hurd YL, Harkany T (2010) Secretagogin is a Ca^{2+}-binding protein identifying prospective extended amygdala neurons in the developing mammalian telencephalon. *Eur J Neurosci* 31: 2166–2177

Nelson MR, Chazin WJ (1998) An interaction-based analysis of calcium-induced conformational changes in Ca^{2+} sensor proteins. *Protein Sci* 7: 270–282

Numazaki M, Tominaga T, Takeuchi K, Murayama N, Toyooka H, Tominaga M (2003) Structural determinant of TRPV1 desensitization interacts with calmodulin. *Proc Natl Acad Sci USA* 100: 8002–8006

Pfeifer MA, Halter JB, Porte D Jr (1981) Insulin secretion in diabetes mellitus. *Am J Med* 70: 579–588

Qian F, Huang P, Ma L, Kuznetsov A, Tamarina N, Philipson LH (2002) TRP genes: candidates for nonselective cation channels and store-operated channels in insulin-secreting cells. *Diabetes* 51(Suppl. 1): S183–S189

Rappsilber J, Mann M, Ishihama Y (2007) Protocol for micro-purification, enrichment, pre-fractionation and storage of peptides for proteomics using StageTips. *Nat Protoc* 2: 1896–1906

Rasmusen CD, Means AR (1990) Effects of changes in calmodulin levels on cell proliferation. *Environ Health Perspect* 84: 31–34

Riera CE, Huising MO, Follett P, Leblanc M, Halloran J, Van AR, de Magalhaes Filho CD, Merkwirth C, Dillin A (2014) TRPV1 pain receptors regulate longevity and metabolism by neuropeptide signaling. *Cell* 157: 1023–1036

Rogstam A, Linse S, Lindqvist A, James P, Wagner L, Berggard T (2007) Binding of calcium ions and SNAP-25 to the hexa EF-hand protein secretagogin. *Biochem J* 401: 353–363

Romanov RA, Alpar A, Zhang MD, Zeisel A, Calas A, Landry M, Fuszard M, Shirran SL, Schnell R, Dobolyi A, Olah M, Spence L, Mulder J, Martens H, Palkovits M, Uhlen M, Sitte HH, Botting CH, Wagner L, Linnarsson S, *et al* (2015) A secretagogin locus of the mammalian hypothalamus controls stress hormone release. *EMBO J* 34: 36–54

Rorsman P, Trube G (1986) Calcium and delayed potassium currents in mouse pancreatic beta-cells under voltage-clamp conditions. *J Physiol* 374: 531–550

Ross RA, Gibson TM, Brockie HC, Leslie M, Pashmi G, Craib SJ, Di Marzo V, Pertwee RG (2001) Structure-activity relationship for the endogenous cannabinoid, anandamide, and certain of its analogues at vanilloid receptors in transfected cells and vas deferens. *Br J Pharmacol* 132: 631–640

Rossi F, Bellini G, Luongo L, Torella M, Mancusi S, De Petrocellis L, Petrosino S, Siniscalco D, Orlando P, Scafuro M, Colacurci N, Perrotta S, Nobili B, Di Marzo V, Maione S (2011) The endovanilloid/endocannabinoid system: a new potential target for osteoporosis therapy. *Bone* 48: 997–1007

Sanz-Salvador L, ndres-Borderia A, Ferrer-Montiel A, Planells-Cases R (2012) Agonist- and Ca^{2+}-dependent desensitization of TRPV1 channel targets the receptor to lysosomes for degradation. *J Biol Chem*, 287: 19462–19471

Schwaller B (2010) Cytosolic Ca^{2+} buffers. *Cold Spring Harb Perspect Biol* 2: a004051

Schwickart M, Huang X, Lill JR, Liu J, Ferrando R, French DM, Maecker H, O'Rourke K, Bazan F, Eastham-Anderson J, Yue P, Dornan D, Huang DC, Dixit VM (2010) Deubiquitinase USP9X stabilizes MCL1 and promotes tumour cell survival. *Nature* 463: 103–107

Segerstolpe A, Palasantza A, Eliasson P, Andersson EM, Andreasson AC, Sun X, Picelli S, Sabirsh A, Clausen M, Bjursell MK, Smith DM, Kasper M, Ammala C, Sandberg R (2016) Single-cell transcriptome profiling of human pancreatic islets in health and type 2 diabetes. *Cell Metab* 24: 593–607

Shen X, Li H, Ou Y, Tao W, Dong A, Kong J, Ji C, Yu S (2008) The secondary structure of calcineurin regulatory region and conformational change induced by calcium/calmodulin binding. *J Biol Chem* 283: 11407–11413

Shirakawa J, Togashi Y, Sakamoto E, Kaji M, Tajima K, Orime K, Inoue H, Kubota N, Kadowaki T, Terauchi Y (2013) Glucokinase activation ameliorates ER stress-induced apoptosis in pancreatic beta-cells. *Diabetes* 62: 3448–3458

Skarnes WC, Rosen B, West AP, Koutsourakis M, Bushell W, Iyer V, Mujica AO, Thomas M, Harrow J, Cox T, Jackson D, Severin J, Biggs P, Fu J, Nefedov M, de Jong PJ, Stewart AF, Bradley A (2011) A conditional knockout resource for the genome-wide study of mouse gene function. *Nature* 474: 337–342

Skovhus KV, Bergholdt R, Erichsen C, Sparre T, Nerup J, Karlsen AE, Pociot F (2006) Identification and characterization of secretagogin promoter activity. *Scand J Immunol* 64: 639–645

Skrzypski M, Khajavi N, Mergler S, Szczepankiewicz D, Kolodziejski PA, Metzke D, Wojciechowicz T, Billert M, Nowak KW, Strowski MZ (2015) TRPV6 channel modulates proliferation of insulin secreting INS-1E beta cell line. *Biochim Biophys Acta* 1853: 3202–3210

Smidak R, Mayer RL, Bileck A, Gerner C, Mechtcheriakova D, Stork O, Lubec G, Li L (2016) Quantitative proteomics reveals protein kinases and phosphatases in the individual phases of contextual fear conditioning in the C57BL/6J mouse. *Behav Brain Res* 303: 208–217

Soleimanpour SA, Crutchlow MF, Ferrari AM, Raum JC, Groff DN, Rankin MM, Liu C, De Leon DD, Naji A, Kushner JA, Stoffers DA (2010) Calcineurin signaling regulates human islet {beta}-cell survival. *J Biol Chem* 285: 40050–40059

Starowicz KM, Cristino L, Matias I, Capasso R, Racioppi A, Izzo AA, Di Marzo V (2008) Endocannabinoid dysregulation in the pancreas and adipose tissue of mice fed with a high-fat diet. *Obesity (Silver Spring)* 16: 553–565

van der Stelt M, Trevisani M, Vellani V, De Petrocellis L, Schiano MA, Campi B, McNaughton P, Geppetti P, Di Marzo V (2005) Anandamide acts as an intracellular messenger amplifying Ca^{2+} influx via TRPV1 channels. *EMBO J* 24: 3026–3037

Sugawara T, Kano F, Murata M (2014) Rab2A is a pivotal switch protein that promotes either secretion or ER-associated degradation of (pro)insulin in insulin-secreting cells. *Sci Rep* 4: 6952

Suriben R, Kaihara KA, Paolino M, Reichelt M, Kummerfeld SK, Modrusan Z, Dugger DL, Newton K, Sagolla M, Webster JD, Liu J, Hebrok M, Dixit VM (2015) beta-cell insulin secretion requires the ubiquitin ligase COP1. *Cell* 163: 1457–1467

Suzuki Y, Nakabayashi Y, Takahashi R (2001) Ubiquitin-protein ligase activity of X-linked inhibitor of apoptosis protein promotes proteasomal degradation of caspase-3 and enhances its anti-apoptotic effect in Fas-induced cell death. *Proc Natl Acad Sci USA* 98: 8662–8667

Tamarina NA, Roe MW, Philipson L (2014) Characterization of mice expressing Ins1 gene promoter driven CreERT recombinase for conditional gene deletion in pancreatic beta-cells. *Islets* 6: e27685

Trinidad AG, Muller PA, Cuellar J, Klejnot M, Nobis M, Valpuesta JM, Vousden KH (2013) Interaction of p53 with the CCT complex promotes protein folding and wild-type p53 activity. *Mol Cell* 50: 805–817

Wagner L, Oliyarnyk O, Gartner W, Nowotny P, Groeger M, Kaserer K, Waldhausl W, Pasternack MS (2000) Cloning and expression of secretagogin, a novel neuroendocrine- and pancreatic islet of Langerhans-specific Ca^{2+}-binding protein. *J Biol Chem* 275: 24740–24751

Wisniewski JR, Zougman A, Nagaraj N, Mann M (2009) Universal sample preparation method for proteome analysis. *Nat Methods* 6: 359–362

Yan J, Zhong N, Liu G, Chen K, Liu X, Su L, Singhal S (2014) Usp9x- and Noxa-mediated Mcl-1 downregulation contributes to pemetrexed-induced apoptosis in human non-small-cell lung cancer cells. *Cell Death Dis* 5: e1316

Yang SY, Lee JJ, Lee JH, Lee K, Oh SH, Lim YM, Lee MS, Lee KJ (2016) Secretagogin impacts insulin secretion in pancreatic beta cells by regulating actin dynamics and focal adhesion. *Biochem J* 437: 1791–1803

Yu W, Niwa T, Miura Y, Horio F, Teradaira S, Ribar TJ, Means AR, Hasegawa Y, Senda T, Niki I (2002) Calmodulin overexpression causes Ca$^{(2+)}$-dependent apoptosis of pancreatic beta cells, which can be prevented by inhibition of nitric oxide synthase. *Lab Invest* 82: 1229–1239

Zhao L, Zhang X, Kuang H, Wu J, Guo Y, Ma L (2013) Effect of TRPV1 channel on the proliferation and apoptosis in asthmatic rat airway smooth muscle cells. *Exp Lung Res* 39: 283–294

Zsombok A, Bhaskaran MD, Gao H, Derbenev AV, Smith BN (2011) Functional plasticity of central TRPV1 receptors in brainstem dorsal vagal complex circuits of streptozotocin-treated hyperglycemic mice. *J Neurosci* 31: 14024–14031